


Exceptional-point-engineered dispersive readout of a driven three-level atom weakly interacting with coupled cavities in non-Markovian environments

J. F. Yang¹ and H. Z. Shen^{1,2,*}¹Center for Quantum Sciences and School of Physics, Northeast Normal University, Changchun 130024, China²Center for Advanced Optoelectronic Functional Materials Research and Key Laboratory for UV Light-Emitting Materials and Technology, Ministry of Education, Northeast Normal University, Changchun 130024, China
 (Received 23 May 2023; revised 17 February 2024; accepted 22 April 2024; published 16 May 2024)

In this paper we study the dispersive readout of a driven three-level atom weakly interacting with a passive cavity that couples to an active cavity. The system excluding the three-level atom exhibits a parity-time (\mathcal{PT}) symmetric phase transition at the exceptional point (EP), which originates from the balance between dissipation of the passive cavity and gain of the active cavity. The perturbation to the passive cavity induced by the three-level atom can be amplified near the EP, where the eigenvalues of the effective Hamiltonian have significant differences when the three-level atom is in the excited, metastable, and ground states, respectively. Applying the modified Laplace transformation and input-output theory near the EP, we can realize the dispersive readout of the three-level atom weakly interacting with coupled cavities, which can be characterized through the different distributions of the transmission spectrum of the passive cavity and the ratio of the active cavity excitation number to the input photon number corresponding to the different levels of the three-level atom. Moreover, we generalize the dispersive readout method to the non-Markovian regime, which is in good agreement with that obtained by the Markovian approximation. We find that the non-Markovian effects of the environment backacting on the system dynamics can lead to the enhancement of the dispersive readout for the three-level atom, which is revealed by the excitation backflow generated in the interaction between the passive cavity and environment. The dispersive readout proposed is conducive to understanding the influences of \mathcal{PT} symmetry and the non-Markovian effect on dispersive readout, which offers the possibility of an alternative field of possible applications for quantum information and quantum communication.

DOI: [10.1103/PhysRevA.109.053712](https://doi.org/10.1103/PhysRevA.109.053712)

I. INTRODUCTION

The basic tasks in quantum information processing are to store, manipulate, and readout the quantum states of the quantum system [1–3]. A nondestructive measurement can be realized in the dispersive regime for the readout of quantum states of a qubit when it is strongly coupled to a cavity system [4–15]. Owing to the interaction between the qubit and cavity, frequency shifts depending on the states of the qubit [4,16] occur for the cavity, which can be used to dispersively read out the quantum states of the qubit via probing experimentally the cavity transmission and reflection [4,17]. The frequency shifts can be obtained to infer the states of the qubit after transforming the qubit-cavity Hamiltonian to the dispersive frame [4], which is usually performed within the rotating-wave approximation (RWA). The dispersive readout has been applied to various systems, such as the quantum circuits [18–39], semiconductor quantum dots [40–49], solid-state spin sensors [50], spin ensembles [51], room-temperature spin qubits [52], molecular spin qubits [53], micromechanical resonators [54], periodically driven quantum systems [55–57], cavity-coupled atoms [58,59], time-dependent systems [60,61], Majorana fermions

in a cavity [62], nonlinear resonators [63–66], nanoelectronic devices [67], superconducting quantum interference devices [68–74], qubit readout [75–107], Majorana qubits [108,109], superconducting artificial atoms [110–114], and multilevel systems within the rotating-wave approximation [115,116]. Moreover, the dispersive readout has been extended to the ultrastrong-coupling [117–120], deep strong-coupling [121], and non-RWA regimes [56,118,122–125]. However, it is still difficult to achieve the dispersive readout method for some other systems remaining in the weak-coupling regimes [8,9], such as a single electron spin coupled to a cavity.

The boundaries of application of cavity spintronics have been developed with the realizations of the cavity-mediated dissipative magnon-magnon coupling [126,127], cavity-magnon coupling [128–130], and dissipative magnon-photon [131–138] coupling in the cavity and magnon-photon entanglement [139]. The quantum state readout of a weakly coupled qubit has been proposed [140] by using a single two-dimensional square superconducting cavity with a pair of nearly resonant modes, where both cavity modes couple to the external probe field but only one of the modes is weakly coupled to the superconducting qubit. In circuit quantum electrodynamics, the one-dimensional superconducting cavity is more commonly used than the two-dimensional superconducting cavity, which can produce a smaller effective volume to achieve a stronger coupling strength. Moreover,

*Corresponding author: shenhz458@nenu.edu.cn

the dissipation of the qubit is neglected in Ref. [140], but the decay rate of the qubit is comparable to the frequency detuning between the qubit and cavity mode in the considered weak-coupling regime, which cannot be ignored directly. In another way, one can measure the states of the weakly coupled system by exploiting the balanced gain and dissipation from two coupled cavities [16,141], which leads to the parity-time (\mathcal{PT}) symmetry. The system with the \mathcal{PT} symmetry has a non-Hermitian Hamiltonian, but there are real energy spectra in the \mathcal{PT} -symmetric phase [142–145]. A phase transition occurs in the parameter space [146–149] by varying the parameters, where the eigenfunctions and eigenvalues of the system can be revealed [132,134,150] at the critical point, i.e., the exceptional point (EP). There are various interesting properties near the EP, such as the enhanced mechanical cooling [151], spontaneous emission [152], lowering of chaos threshold power [153], unidirectional invisibility [153–155], and lasing [156–158]. In particular, the sensitivity of the dispersive readout can be enhanced near the EP in metrology [159,160] and microcavity sensors [161].

With the rapid development of quantum information technology [1,162], open quantum systems [163,164] have attracted increasing attention. In general, all the quantum systems in reality are open owing to the unavoidable coupling with the environments [165–168]. The Markovian approximation for open systems [163,164] is only valid when the coupling between the system and environment is weak and the characteristic times of the system under study are adequately longer than those of the bath. Otherwise we should take the non-Markovian effects interacting with the system dynamics [169] into account, which occur in many quantum systems including coupled cavities [170], photonic crystals [171], colored noises [172], cavities coupled to waveguides [173,174], and implementation in experiment [175–182]. The non-Markovian process proves to be useful in quantum information processing including quantum state engineering, quantum control, and quantum channel capacity [183,184]. The non-Markovian effects of the environments backacting on the system dynamics can be characterized by the excitation backflowing between the system and its environment [185–188], which leads to different measures of non-Markovianity [189,190].

However, several questions naturally arise. (i) How is the dispersive readout of the three-level atom realized in the weak-coupling regime? (ii) Is it effective to generalize the dispersive readout in Markovian systems to non-Markovian ones? (iii) How can non-Markovian effects influence the dispersive readout? To address these questions, we propose a scheme to realize the dispersive readout of the driven three-level atom weakly interacting with a passive cavity that couples to an active cavity. When the dissipation of the passive cavity can be compensated exactly by the gain from the active cavity [159,160], the real and imaginary parts of the eigenvalues coalesce at the EP. The sensitivity of the dispersive readout is highly enhanced near the EP, which contributes to the dispersive readout of the excited, metastable, and ground states of the three-level atom via the different transmissions of the passive cavity corresponding to the different levels of the three-level atom. Moreover, we generalize the method to the case with the non-Markovian environment, which can

return to the Markovian results in the wideband limit. We point out that the influence of the non-Markovian effects reacting on the system dynamics can enhance the dispersive readout of the three-level atom. Compared with the ground and excited states, the metastable state of the three-level atom can be dispersively read out when the environmental spectrum width is small. As the environmental spectrum width increases, the relative heights of the two peaks of the transmission spectrum of the passive cavity and the ratio of the active cavity excitation number to the input photon number change significantly when the three-level atom is in the excited state.

The remainder of the paper is organized as follows. In Sec. II the model and Hamiltonian are described for dispersive readout of the driven three-level atom weakly interacting with a passive cavity that couples to an active cavity. In Sec. III we discuss the influence of the existence or absence of the EP on the dispersive readout of the three-level atom through the different transmission spectra of the passive cavity and the ratio of the active cavity excitation number to the input photon number corresponding to the different levels of the three-level atom. In Sec. IV we generalize the dispersive readout theory to the non-Markovian regime. In Sec. V we study the dispersive readout of the three-level atom with the non-Markovian effects and compare it with that obtained by the Markovian approximation. We summarize and discuss our results in Sec. VI.

II. DISPERSIVE READOUT UNDER THE MARKOVIAN APPROXIMATION

A. Frequency shifts of the passive cavity induced by the three-level atom

We construct a coupled-cavity system to realize the dispersive readout of the three-level atom driven by a classical driving field (strength Ω and frequency ω_l) between excited state $|x\rangle$ and metastable state $|e\rangle$ in Fig. 1, where the transition from $|g\rangle$ to $|x\rangle$ is mediated by the passive cavity with coupling constant g . The Hamiltonian with the three-level atom and coupled cavities reads

$$\begin{aligned} \hat{H} = & \omega_a \hat{a}^\dagger \hat{a} + \omega_b \hat{b}^\dagger \hat{b} + \omega_x \hat{\sigma}_{xx} + \omega_e \hat{\sigma}_{ee} + \omega_g \hat{\sigma}_{gg} \\ & + \Omega(e^{i\omega_l t} \hat{\sigma}_{ex} + e^{-i\omega_l t} \hat{\sigma}_{xe}) + g(\hat{\sigma}_{xg} \hat{a} + \hat{\sigma}_{gx} \hat{a}^\dagger) \\ & + G(\hat{a}^\dagger \hat{b} + \hat{b}^\dagger \hat{a}), \end{aligned} \quad (1)$$

where \hat{a} and \hat{b} denote annihilation operators of the passive cavity (eigenfrequency ω_a) and active cavity (eigenfrequency ω_b), respectively; G represents the coupling strength between the passive cavity and active cavity; ω_x , ω_e , and ω_g are the energy-level frequencies of the excited, metastable, and ground states of the three-level atom, respectively; and $\hat{\sigma}_{ex}$, $\hat{\sigma}_{xe}$, $\hat{\sigma}_{xg}$, and $\hat{\sigma}_{gx}$ denote the transition operators of the three-level atom [191,192], e.g., $\hat{\sigma}_{nm} = |n\rangle\langle m|$ describes the transition between level $|n\rangle$ and level $|m\rangle$. In a rotating frame defined by the unitary transformation $\hat{U} = \exp[-i\frac{\omega_l}{2}\hat{a}^\dagger \hat{a} t - i\frac{\omega_l}{2}(\hat{\sigma}_{xx} - \hat{\sigma}_{ee})t]$ with $\omega_l = 2\omega_a$, the Hamiltonian (1) becomes

$$\hat{H} = \hat{H}_{aa} + \hat{H}_{ab}, \quad (2)$$

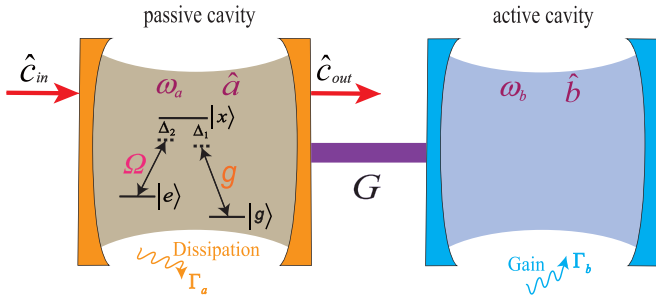


FIG. 1. Illustration of the setup for the dispersive readout of a driven three-level atom weakly interacting with a passive cavity (eigenfrequency ω_a and dissipation Γ_a). The active cavity (eigenfrequency ω_b and gain Γ_b) couples to the passive cavity via coupling strength G [159,160]. The atom weakly coupled to the passive cavity with the coupling strength g has three relevant electronic levels, i.e., the excited state $|x\rangle$, metastable state $|e\rangle$, and ground state $|g\rangle$. The transition from level $|e\rangle$ to level $|x\rangle$ is driven by the classical driving field with strength Ω and frequency ω_l . The \hat{c}_{in} and \hat{c}_{out} denote the input-field and output-field operators, respectively. The passive cavity and classical driving field are detuned from the three-level atom and are denoted by Δ_1 and Δ_2 , respectively. The scheme might also be implemented by a driven three-level atom weakly interacting with the cavity-magnon system in Appendix A.

with

$$\begin{aligned}\hat{H}_{aa} &= \tilde{\omega}_x \hat{\sigma}_{xx} + \tilde{\omega}_e \hat{\sigma}_{ee} + \omega_g \hat{\sigma}_{gg} + \Omega(\hat{\sigma}_{ex} + \hat{\sigma}_{xe}) \\ &\quad + g(\hat{\sigma}_{xg} \hat{a} + \hat{\sigma}_{gx} \hat{a}^\dagger), \\ \hat{H}_{ab} &= \Delta_b \hat{b}^\dagger \hat{b} + G(\hat{a}^\dagger \hat{b} + \hat{b}^\dagger \hat{a}),\end{aligned}\quad (3)$$

where $\tilde{\omega}_x = \omega_x - \omega_a$, $\tilde{\omega}_e = \omega_e + \omega_a$, and $\Delta_b = \omega_b - \omega_a$. To obtain the Hamiltonian under the dispersive condition, we can perform the Schrieffer-Wolff transformation [53,58,193] to Eq. (2) as $\hat{H}_{SW1} = e^{\hat{s}_1} \hat{H} e^{-\hat{s}_1} = e^{\hat{s}_1} \hat{H}_{ab} e^{-\hat{s}_1} + e^{\hat{s}_1} \hat{H}_{aa} e^{-\hat{s}_1} = e^{\hat{s}_1} \hat{H}_{ab} e^{-\hat{s}_1} + \hat{H}_{aa} + [\hat{s}_1, \hat{H}_{aa}] + \frac{1}{2}[\hat{s}_1, [\hat{s}_1, \hat{H}_{aa}]] + \dots$, with $\hat{H}_{aa} = \hat{h}_1 + \hat{v}_1$ via $\hat{h}_1 = \tilde{\omega}_x \hat{\sigma}_{xx} + \tilde{\omega}_e \hat{\sigma}_{ee} + \omega_g \hat{\sigma}_{gg}$ and $\hat{v}_1 = \Omega(\hat{\sigma}_{ex} + \hat{\sigma}_{xe}) + g(\hat{\sigma}_{xg} \hat{a} + \hat{\sigma}_{gx} \hat{a}^\dagger)$, where \hat{s}_1 is the transformation generator and has anti-Hermitian properties. Taking

$$\hat{s}_1 = \frac{g}{\Delta_1} (\hat{\sigma}_{xg} \hat{a} - \hat{\sigma}_{gx} \hat{a}^\dagger) - \frac{\Omega}{\Delta_2} (\hat{\sigma}_{ex} - \hat{\sigma}_{xe}) \quad (4)$$

satisfies $[\hat{h}_1, \hat{s}_1] = \hat{v}_1$, which can approximate \hat{H}_{SW1} to first order in g/Δ_1 and Ω/Δ_2 in the dispersive regime $g \ll |\Delta_1|$ and $\Omega \ll |\Delta_2|$ [126,194], where $\Delta_1 = \tilde{\omega}_x - \omega_g = \omega_x - \omega_a - \omega_g$ and $\Delta_2 = \tilde{\omega}_e - \omega_l = \omega_e - \omega_a - \omega_l$ are two detunings of the passive cavity and driving field with respect to the three-level atom, respectively. In this case, we have $\hat{H}_{SW1} = e^{\hat{s}_1} \hat{H}_{ab} e^{-\hat{s}_1} + \hat{h}_1 + \frac{1}{2}[\hat{s}_1, \hat{v}_1] + O(g^2/\Delta_1^2, \Omega^2/\Delta_2^2)$, which leads to

$$\begin{aligned}\hat{H}_{SW1} &= e^{\hat{s}_1} \hat{H}_{ab} e^{-\hat{s}_1} + \hat{h}_1 + \frac{g^2}{\Delta_1} (\hat{\sigma}_{xx} \hat{a} \hat{a}^\dagger - \hat{\sigma}_{gg} \hat{a}^\dagger \hat{a}) \\ &\quad - \frac{g\Omega}{\Delta} (\hat{\sigma}_{eg} \hat{a} + \hat{\sigma}_{ge} \hat{a}^\dagger) + \frac{\Omega^2}{\Delta_2} (\hat{\sigma}_{xx} - \hat{\sigma}_{ee}) \\ &\equiv e^{\hat{s}_1} \hat{H}_{ab} e^{-\hat{s}_1} + \hat{h}_2 + \hat{v}_2,\end{aligned}\quad (5)$$

where $\hat{h}_2 = \hat{h}_1 + \frac{g^2}{\Delta_1} (\hat{\sigma}_{xx} \hat{a} \hat{a}^\dagger - \hat{\sigma}_{gg} \hat{a}^\dagger \hat{a}) + \frac{\Omega^2}{\Delta_2} (\hat{\sigma}_{xx} - \hat{\sigma}_{ee})$, $\hat{v}_2 = -\frac{g\Omega}{\Delta} (\hat{\sigma}_{eg} \hat{a} + \hat{\sigma}_{ge} \hat{a}^\dagger)$, and $\bar{\Delta} = 2\Delta_1 \Delta_2 / (\Delta_1 + \Delta_2)$. With Eq. (5) and choosing $\hat{s}_2 = -g\Omega(\hat{\sigma}_{eg} \hat{a} - \hat{\sigma}_{ge} \hat{a}^\dagger) / \bar{\Delta}(\Delta_1 - \Delta_2)$, meeting $[\hat{h}_2, \hat{s}_2] = \hat{v}_2$ under the condition $g\Omega \ll |\bar{\Delta}(\Delta_1 - \Delta_2)|$, we get

$$\begin{aligned}\hat{H}_{SW2} &= e^{\hat{s}_2} \hat{H}_{SW1} e^{-\hat{s}_2} \\ &\approx e^{\hat{s}_2} e^{\hat{s}_1} \hat{H}_{ab} e^{-\hat{s}_1} e^{-\hat{s}_2} + \hat{h}_2 + \frac{1}{2}[\hat{s}_2, \hat{v}_2] \\ &\quad + O(g^2 \Omega^2 / |\bar{\Delta}|^2 / |\Delta_1 - \Delta_2|^2),\end{aligned}\quad (6)$$

and then

$$\hat{H}_{SW2} = \hat{\mathcal{H}}_{ab} + \hat{\mathcal{H}}_{aa}, \quad (7)$$

with

$$\hat{\mathcal{H}}_{ab} = e^{\hat{s}_2} e^{\hat{s}_1} \hat{H}_{ab} e^{-\hat{s}_1} e^{-\hat{s}_2}, \quad (8)$$

$$\begin{aligned}\hat{\mathcal{H}}_{aa} &= \left[\frac{g^2}{\Delta_1} \hat{\sigma}_{xx} + \frac{g^2 \Omega^2}{\bar{\Delta}^2 (\Delta_1 - \Delta_2)} \hat{\sigma}_{ee} \right. \\ &\quad \left. - \left(\frac{g^2}{\Delta_1} + \frac{g^2 \Omega^2}{\bar{\Delta}^2 (\Delta_1 - \Delta_2)} \right) \hat{\sigma}_{gg} \right] \hat{a}^\dagger \hat{a} \\ &\quad + \left(\tilde{\omega}_x + \frac{g^2}{\Delta_1} + \frac{\Omega^2}{\Delta_2} \right) \hat{\sigma}_{xx} + \omega_g \hat{\sigma}_{gg} \\ &\quad + \left(\tilde{\omega}_e - \frac{\Omega^2}{\Delta_2} + \frac{g^2 \Omega^2}{\bar{\Delta}^2 (\Delta_1 - \Delta_2)} \right) \hat{\sigma}_{ee},\end{aligned}\quad (9)$$

which are valid under the dispersive condition

$$g \ll |\Delta_1|, \quad \Omega \ll |\Delta_2|, \quad g\Omega \ll |\bar{\Delta}(\Delta_1 - \Delta_2)|. \quad (10)$$

B. Validating the parameters by neglecting the perturbative terms in Eq. (8)

We now study the influence of the anti-Hermitian operators \hat{s}_1 and \hat{s}_2 on $\hat{\mathcal{H}}_{ab}$ in Eq. (8). Under the dispersive condition (10), we can expand $\hat{\mathcal{H}}_{ab}$ of Eq. (8) in powers of g/Δ_1 or Ω/Δ_2 , whose first few terms are

$$\begin{aligned}\hat{\mathcal{H}}_{ab} &= \hat{H}_{ab} + G \frac{g}{\Delta_1} (\hat{\sigma}_{xg} \hat{b} + \hat{b}^\dagger \hat{\sigma}_{gx}) \\ &\quad + G \frac{g^2}{2\Delta_1^2} (\hat{\sigma}_{xx} - \hat{\sigma}_{gg}) (\hat{a}^\dagger \hat{b} + \hat{b}^\dagger \hat{a}) \\ &\quad - G \left(\frac{g\Omega}{\Delta_2 (\Delta_1 - \Delta_2)} \right) (\hat{\sigma}_{eg} \hat{b} + \hat{b}^\dagger \hat{\sigma}_{ge}) \\ &\quad - G \frac{g\Omega^2}{6\Delta_1 \Delta_2^2} (\hat{\sigma}_{gx} \hat{b}^\dagger + \hat{\sigma}_{xg} \hat{b}) \\ &\quad - G \frac{g^2 \Omega}{6\Delta_1^2 \Delta_2} [\hat{\sigma}_{ex} (2\hat{a}^\dagger \hat{b} + \hat{a} \hat{b}^\dagger) + \hat{\sigma}_{xe} (2\hat{a} \hat{b}^\dagger \\ &\quad + \hat{a}^\dagger \hat{b})] - G \frac{g^3}{6\Delta_1^3} [2\hat{\sigma}_{xg} \hat{a}^2 \hat{b}^\dagger + 2\hat{\sigma}_{gx} \hat{a}^{\dagger 2} \hat{b} \\ &\quad + (\hat{\sigma}_{xg} \hat{b} + \hat{\sigma}_{gx} \hat{b}^\dagger) (\hat{a}^\dagger \hat{a} + \hat{a} \hat{a}^\dagger)] \\ &\quad - G \frac{g^2 \Omega (\Delta_1 + \Delta_2)}{2\Delta_1^2 \Delta_2 (\Delta_1 - \Delta_2)} (\hat{\sigma}_{ex} \hat{a} \hat{b}^\dagger + \hat{\sigma}_{xe} \hat{a}^\dagger \hat{b}) + \dots,\end{aligned}\quad (11)$$

where the ellipsis denotes higher-order terms and \hat{H}_{ab} is given by Eq. (3). If $\hat{\mathcal{H}}_{ab}$ in Eq. (11) can be approximated as \hat{H}_{ab} by neglecting the perturbative terms, Eq. (7) becomes

$$\begin{aligned} \hat{H}_{\text{SW}2} &\approx \hat{H}_{ab} + \hat{\mathcal{H}}_{aa} \\ &= \sum_n \mathcal{C}^{(n)} \hat{\sigma}_{nm} \hat{a}^\dagger \hat{a} + \Delta_b \hat{b}^\dagger \hat{b} + G(\hat{a}^\dagger \hat{b} + \hat{b}^\dagger \hat{a}), \end{aligned} \quad (12)$$

where $n = x, e, g$ and the atom-induced frequency shifts of the passive cavity [5,58,195]

$$\begin{aligned} \mathcal{C}^{(x)} &= \frac{g^2}{\Delta_1}, \quad \mathcal{C}^{(e)} = \frac{g^2 \Omega^2}{\bar{\Delta}^2 (\Delta_1 - \Delta_2)}, \\ \mathcal{C}^{(g)} &= -\frac{g^2}{\Delta_1} - \frac{g^2 \Omega^2}{\bar{\Delta}^2 (\Delta_1 - \Delta_2)}. \end{aligned} \quad (13)$$

Below we discuss the validity of the approximate Hamiltonian (12) compared to the exact Hamiltonian (2). In a single excited subspace with excitation number $\hat{N} = \hat{a}^\dagger \hat{a} + \hat{b}^\dagger \hat{b} + \hat{\sigma}_{xx} + \hat{\sigma}_{ee}$ conserved due to $[\hat{H}, \hat{N}] = 0$, we write the state by Eq. (2) at time t as

$$\begin{aligned} |\varphi(t)\rangle &= c_x(t)|x, 0, 0\rangle + c_e(t)|e, 0, 0\rangle \\ &\quad + c_a(t)|g, 1, 0\rangle + c_b(t)|g, 0, 1\rangle, \end{aligned} \quad (14)$$

where $|g, 1, 0\rangle$ represents the state of the atom in the ground state $|g\rangle$ with one photon in the passive cavity and no photon in the active cavity and $c_a(t)$ denotes the probability amplitude of the system being in the state $|g, 1, 0\rangle$. The other states in Eq. (14) have similar notation. The Schrödinger equation $i\dot{|\varphi(t)\rangle} = \hat{H}|\varphi(t)\rangle$ with Eq. (2) leads to

$$\begin{aligned} i\dot{c}_x(t) &= \tilde{\omega}_x c_x(t) + \Omega c_e(t) + g c_a(t), \\ i\dot{c}_e(t) &= \tilde{\omega}_e c_e(t) + \Omega c_x(t), \\ i\dot{c}_a(t) &= \omega_g c_a(t) + g c_x(t) + G c_b(t), \\ i\dot{c}_b(t) &= \Delta_b c_b(t) + G c_a(t). \end{aligned} \quad (15)$$

For the approximate Hamiltonian given by Eq. (12), the state at time t can be written as

$$|\tilde{\varphi}(t)\rangle = \tilde{c}_a(t)|g, 1, 0\rangle + \tilde{c}_b(t)|g, 0, 1\rangle, \quad (16)$$

where the probability amplitudes satisfying the Schrödinger equation $i\dot{|\tilde{\varphi}(t)\rangle} = \hat{H}_{\text{SW}2}|\tilde{\varphi}(t)\rangle$ are determined by

$$i\dot{\tilde{c}}_a(t) = \mathcal{C}^{(g)} \tilde{c}_a(t) + G \tilde{c}_b(t), \quad i\dot{\tilde{c}}_b(t) = \Delta_b \tilde{c}_b(t) + G \tilde{c}_a(t). \quad (17)$$

In Fig. 2 we show that $|\tilde{c}_a(t)|^2$ and $|\tilde{c}_b(t)|^2$ given by Eq. (17) with the approximate Hamiltonian (12) are in good agreement with $|c_a(t)|^2$ and $|c_b(t)|^2$ obtained by Eq. (15) with the exact Hamiltonian (2) when the parameters take values $g = 0.05\Gamma_a$, $\Omega = 0.1\Gamma_a$, $\Delta_1 = \Gamma_a$, and $\Delta_2 = -2\Gamma_a$ [satisfying Eq. (10)]. In this case, we point out that the three-level atom remains in its initial state due to the weak atom-cavity coupling strength $g = 0.05\Gamma_a$, while coupled cavities remain in the vacuum state or exhibit periodic equal-amplitude oscillations due to the large coupling strength $G = 0.5\Gamma_a$ between the passive cavity and active cavity. To be specific, the probability $|c_a(t)|^2 + |c_b(t)|^2$ of the three-level atom being in the ground state is approximately 1 for the initial state $|g, 1, 0\rangle$ in Figs. 2(a) and

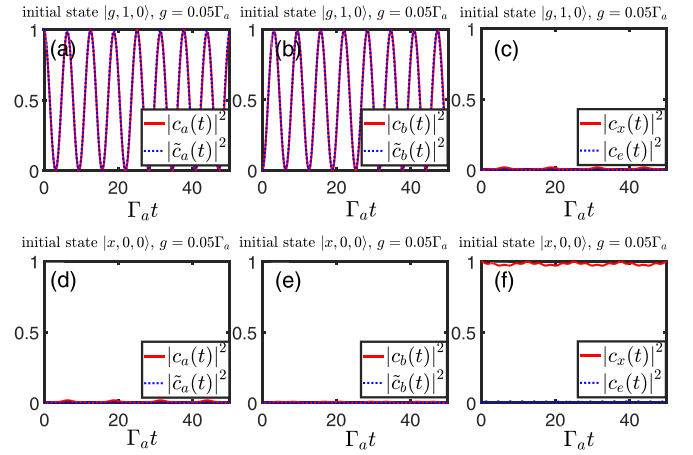


FIG. 2. Time evolution of the probabilities determined by Eqs. (15) and (17), corresponding to the exact Hamiltonian (2) and approximate Hamiltonian (12), respectively, with fixed atom-cavity coupling strength $g = 0.05\Gamma_a$. The initial states are (a)–(c) $|g, 1, 0\rangle$ and (d)–(f) $|x, 0, 0\rangle$. The parameters are $\Omega = 0.1\Gamma_a$, $G = 0.5\Gamma_a$, $\Delta_b = 0$, $\tilde{\omega}_x = 1.2\Gamma_a$, $\tilde{\omega}_e = 3.2\Gamma_a$, and $\omega_g = 0.2\Gamma_a$, corresponding to $\Delta_1 = \Gamma_a$ and $\Delta_2 = -2\Gamma_a$.

2(b), while $|c_a(t)|^2$ and $|c_b(t)|^2$ in coupled cavities behave like periodic equal-amplitude oscillations. This indicates that Eqs. (12) and (17) are valid under the given parameters given in Fig. 2 and the presence of the three-level atom has almost no influence on the dynamics of coupled cavities. If the initial state is prepared in the state $|x, 0, 0\rangle$, the three-level atom remains in the state $|x\rangle$ due to $|c_x(t)|^2 \approx 1$ in Fig. 2(f), which leads to coupled cavities holding in the vacuum state $|0, 0\rangle$.

With the increase of atom-cavity coupling strength to $g = 0.2\Gamma_a$ when the other parameters are fixed, $|\tilde{c}_a(t)|^2$ and $|\tilde{c}_b(t)|^2$ in Eq. (17) obtained by the approximate Hamiltonian (12) seriously deviate from $|c_a(t)|^2$ and $|c_b(t)|^2$ in Eq. (15), obtained by the exact Hamiltonian (2) in Figs. 3(a), 3(b), 3(d), and 3(e).

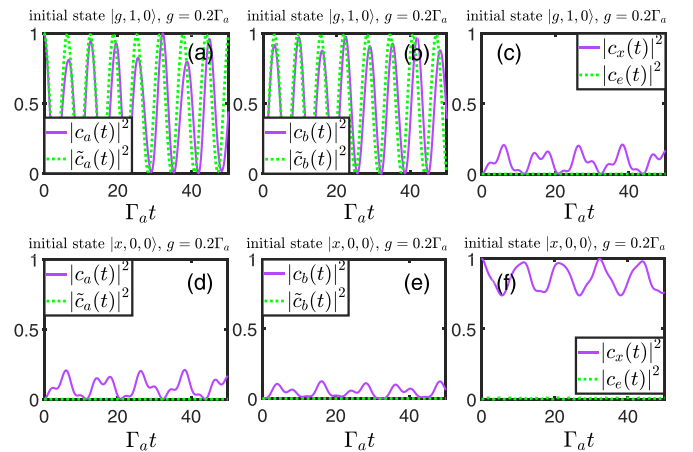


FIG. 3. Plots showing that the results in Eq. (17) obtained by the approximate Hamiltonian (12) seriously deviate from those in Eq. (15) obtained by the exact Hamiltonian (2) with the increase of atom-cavity coupling strength to $g = 0.2\Gamma_a$. The other parameters are the same as those in Fig. 2.

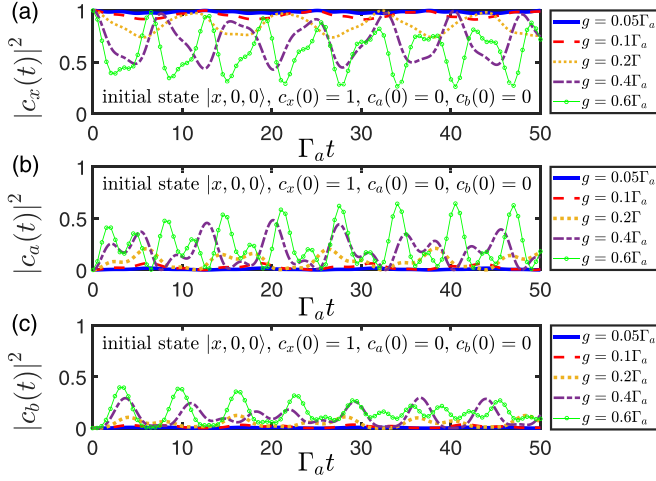


FIG. 4. The $|c_x(t)|^2$, $|c_a(t)|^2$, and $|c_b(t)|^2$ determined by Eq. (15), corresponding to the exact Hamiltonian (2), vary over time t with different atom-cavity coupling strength g , where the initial state is $|x, 0, 0\rangle$. The other parameters are the same as those in Fig. 2.

In this case, the three-level-atom states no longer remain in the initial state, i.e., $|c_x(t)|^2 + |c_b(t)|^2 \neq 1$ [purple solid line in Figs. 3(a) and 3(b)] and $|c_x(t)|^2 \neq 1$ [purple solid line in Fig. 3(f)], and the probabilities in coupled cavities do not exhibit periodic equal-amplitude oscillations [see the purple solid line in Figs. 3(a) and 3(b)]. This means that the presence of the three-level atom has a large influence on the dynamics of coupled cavities, which results in Eqs. (12) and (17) being invalid for the given parameters in Fig. 3. Further observations can also be found in Fig. 4 with different atom-cavity coupling strength g when the initial state is $|x, 0, 0\rangle$.

Based on the above discussion, we use the valid parameters in Fig. 2 to study the dispersive readout of a driven three-level atom weakly interacting with coupled cavities in the following sections.

C. Measuring the frequency shifts by the passive cavity interacting with the active cavity

Considering dissipation of the passive cavity and gain of the active cavity, the Hamiltonian in Eq. (12) reads [159,160]

$$\hat{H}_M = \left(\sum_n C^{(n)} \hat{\sigma}_{nm} - i \frac{\Gamma_a}{2} \right) \hat{a}^\dagger \hat{a} + G(\hat{a}^\dagger \hat{b} + \hat{b}^\dagger \hat{a}) + \left(\Delta_b + i \frac{\Gamma_b}{2} \right) \hat{b}^\dagger \hat{b}, \quad (18)$$

where Γ_a and Γ_b denote the dissipation and gain of the passive cavity and active cavity, respectively. In the following discussion, Δ_1 and Δ_2 of $C^{(n)}$ in Eq. (18) are replaced by $\Delta_1 - i\gamma_1$ and $\Delta_2 - i\gamma_2$ through introducing the dissipations γ_1 and γ_2 of the three-level atom. The corresponding eigenfrequencies in Eq. (18) read $\Delta \hat{E}_\pm = \frac{1}{2} [\sum_n C^{(n)} \hat{\sigma}_{nm} + \Delta_b - i \frac{\Gamma_a}{2} + i \frac{\Gamma_b}{2} \pm \sqrt{4G^2 + (\sum_n C^{(n)} \hat{\sigma}_{nm} - \Delta_b - i \frac{\Gamma_a}{2} - i \frac{\Gamma_b}{2})^2}]$. By inserting the completeness relation $\sum_m |m\rangle \langle m| = I$ ($m = x, e, g$ and I

denotes the identity matrix) into $\Delta \hat{E}_\pm$, we obtain

$$\Delta \hat{E}_\pm = \sum_n \Delta E_\pm^{(n)} |n\rangle \langle n|, \quad (19)$$

with the different distributions corresponding to the different levels of the three-level atom

$$\Delta E_\pm^{(n)} = \frac{1}{2} \left[C^{(n)} + \Delta_b - i \frac{\Gamma_a}{2} + i \frac{\Gamma_b}{2} \pm \sqrt{4G^2 + \left(C^{(n)} - \Delta_b - i \frac{\Gamma_a}{2} - i \frac{\Gamma_b}{2} \right)^2} \right], \quad (20)$$

where the real part of $\Delta E_\pm^{(n)} = E_\pm^{(n)} - \omega_a$ denotes resonant frequencies, while its imaginary part describes the dissipation of the system. The EP corresponding to the situation where the two eigenenergies and their eigenstates coalesce [151,161,196,197] leads to $\Delta_b = 0$ (see Appendix B for more details). With the balance between dissipation of the passive cavity and gain of the active cavity $\Gamma_a = \Gamma_b$, the two eigenfrequencies are reduced to

$$\Delta E_\pm^{(n)} = \frac{1}{2} \left\{ C^{(n)} \pm \sqrt{(C^{(n)})^2 + 4 \left[G^2 - i C^{(n)} \frac{\Gamma_a}{2} - \left(\frac{\Gamma_a}{2} \right)^2 \right]} \right\}. \quad (21)$$

In the absence of the three-level atom ($C^{(n)} = 0$), Eq. (21) gives $\Delta E_\pm^{(n)} = \pm \sqrt{G^2 - \Gamma_a^2/4}$, which indicates that the system has \mathcal{PT} symmetry and two real eigenvalues exist when $G > \Gamma_a/2$ is satisfied, while the \mathcal{PT} -symmetry breaking leads to two complex eigenvalues for $G < \Gamma_a/2$. There is an interesting phenomenon in which the real and imaginary parts of $\Delta E_\pm^{(n)}$ coalesce at $G = \Gamma_a/2$, which results in the balanced dissipation and gain from passive and active cavities. The dispersive readout sensitivity of the frequency or energy splitting can be greatly enhanced near the EP, which motivates us to perform dispersive readout of the weakly coupled system. With these, the condition of the \mathcal{PT} -symmetric phase transition is determined by

$$\Delta_b = 0, \quad G = \frac{\Gamma_a}{2}, \quad \Gamma_a = \Gamma_b, \quad (22)$$

whose derivation can be found in Appendix B.

D. Input-output theory under the Markovian approximation

Here we derive the transmission coefficient of the passive cavity and the ratio of the active cavity excitation number to the input photon number, which can be used to realize the dispersive readout of the weakly coupled system. With Eq. (18), the Heisenberg-Langevin equations under the Markovian approximation are

$$\frac{d}{dt} \hat{a}(t) = -i \left(\sum_n C^{(n)} \hat{\sigma}_{nm} - i \frac{\Gamma_a}{2} \right) \hat{a}(t) - i G \hat{b}(t) + \sqrt{\Gamma_a} \hat{c}_{in}(t), \quad (23)$$

$$\frac{d}{dt} \hat{b}(t) = -i \left(\Delta_b + i \frac{\Gamma_b}{2} \right) \hat{b}(t) - i G \hat{a}(t), \quad (24)$$

where $\hat{\sigma}_{nm}(t) \equiv \hat{\sigma}_{nm}$ is used due to $[\hat{\sigma}_{nm}, \hat{H}_M] = 0$ with Eq. (18), which is a constant of motion [58]. Applying the modified Laplace transformation $\hat{A}(\omega) = \int_0^\infty \hat{a}(t)e^{i\Delta\omega t} dt$ [198–200] to Eqs. (23) and (24) with $\Delta\omega = \omega - \omega_a$, we have

$$\begin{aligned} & \left(\Delta\omega - \sum_n \mathcal{C}^{(n)} \hat{\sigma}_{nm} + i\frac{\Gamma_a}{2} \right) \hat{A}(\omega) - G\hat{\mathcal{M}}(\omega) \\ & - i\sqrt{\Gamma_a} \hat{\mathcal{C}}_{\text{in}}(\omega) = 0, \\ & \left(\Delta\omega - \Delta_b - i\frac{\Gamma_b}{2} \right) \hat{\mathcal{M}}(\omega) - G\hat{A}(\omega) = 0, \end{aligned} \quad (25)$$

which lead to

$$\begin{aligned} \hat{A}(\omega) &= \frac{i\sqrt{\Gamma_a}(\Delta\omega - \Delta_b - i\frac{\Gamma_b}{2})}{\hat{R}(\Delta\omega - \Delta_b - i\frac{\Gamma_b}{2}) - G^2} \hat{\mathcal{C}}_{\text{in}}(\omega), \\ \hat{\mathcal{M}}(\omega) &= \frac{iG\sqrt{\Gamma_a}}{\hat{R}(\Delta\omega - \Delta_b - i\frac{\Gamma_b}{2}) - G^2} \hat{\mathcal{C}}_{\text{in}}(\omega), \end{aligned} \quad (26)$$

where $\hat{R} = \Delta\omega - \sum_n \mathcal{C}^{(n)} \hat{\sigma}_{nm} + i\Gamma_a/2$. The ratio of the active cavity excitation number to the input photon number [201] can be obtained by

$$\hat{V}(\omega) \propto \frac{\hat{\mathcal{M}}^\dagger(\omega)\hat{\mathcal{M}}(\omega)}{\hat{\mathcal{C}}_{\text{in}}^\dagger(\omega)\hat{\mathcal{C}}_{\text{in}}(\omega)} = \left| \frac{iG\sqrt{\Gamma_a}}{\hat{R}(\Delta\omega - \Delta_b - i\frac{\Gamma_b}{2}) - G^2} \right|^2. \quad (27)$$

By inserting the completeness relation $\sum_m |m\rangle\langle m| = I$ into $\hat{V}(\omega)$ in Eq. (27), we obtain

$$\hat{V}(\omega) = \sum_n V^{(n)}(\omega) |n\rangle\langle n|, \quad (28)$$

with the different distributions corresponding to the different levels of the three-level atom

$$V^{(n)}(\omega) = \left| \frac{iG\sqrt{\Gamma_a}}{r_n(\Delta\omega - \Delta_b - i\frac{\Gamma_b}{2}) - G^2} \right|^2, \quad (29)$$

where $r_n = \Delta\omega - \mathcal{C}^{(n)} + i\Gamma_a/2$.

From Eq. (26), $\hat{A}(\omega)$ can be rewritten as

$$\hat{A}(\omega) = \frac{i\sqrt{\Gamma_a} \hat{\mathcal{C}}_{\text{in}}(\omega)}{\Delta\omega - \sum_n \mathcal{C}^{(n)} \hat{\sigma}_{nm} + i\frac{\Gamma_a}{2} - \mathcal{Z}(\omega)}, \quad (30)$$

where the self-energy $\mathcal{Z}(\omega)$ induced by the active cavity is $\mathcal{Z}(\omega) = G^2/(\Delta\omega - \Delta_b - i\Gamma_b/2)$. With the input-output theory

$$\hat{c}_{\text{out}}(t) = \hat{c}_{\text{in}}(t) - \sqrt{\Gamma_a} \hat{a}(t), \quad (31)$$

the intracavity field $\hat{a}(t)$ can be connected by the input field $\hat{c}_{\text{in}}(t)$ and output field $\hat{c}_{\text{out}}(t)$. Making the modified Laplace transformation to Eq. (31) gives $\hat{\mathcal{C}}_{\text{out}}(\omega) = \hat{\mathcal{C}}_{\text{in}}(\omega) - \sqrt{\Gamma_a} \hat{A}(\omega)$. With Eq. (30), we obtain the transmission coefficient of the passive cavity

$$\hat{\mathcal{T}}(\omega) = \frac{\hat{\mathcal{C}}_{\text{out}}(\omega)}{\hat{\mathcal{C}}_{\text{in}}(\omega)} \quad (32)$$

$$= \sum_n \mathcal{T}^{(n)}(\omega) |n\rangle\langle n|, \quad (33)$$

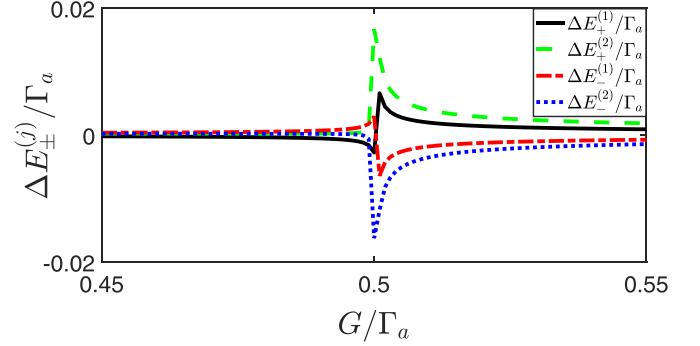


FIG. 5. Eigenfrequency difference $\Delta E_{\pm}^{(j)}/\Gamma_a$ of the effective Hamiltonian (18), as a function of the coupling strength G/Γ_a , solved by Eq. (35), where $\Delta_b = 0$ and $\Gamma_a = \Gamma_b$. The parameters are $g = 0.05\Gamma_a$, $\Omega = 0.1\Gamma_a$, $\Delta_1 = \Gamma_a$, $\Delta_2 = -2\Gamma_a$, and $\gamma_1 = \gamma_2 = 3\Gamma_a$.

with the different distributions corresponding to the different levels of the three-level atom

$$\mathcal{T}^{(n)}(\omega) = 1 - \frac{i\Gamma_a}{\Delta\omega - \mathcal{C}^{(n)} + i\frac{\Gamma_a}{2} - \mathcal{Z}(\omega)}, \quad (34)$$

which can be used to realize the dispersive readout of the three-level atom in the weak-coupling regime. In the process of deriving Eqs. (19), (28), and (33), we use $\hat{\sigma}_{mn}|m\rangle\langle m| = \delta_{mn}|n\rangle\langle n|$, where δ_{mn} represents the Kronecker delta symbol, i.e., $\delta_{mn} = 1$ for $m = n$ while $\delta_{mn} = 0$ for $m \neq n$. From Eqs. (28) and (33) we show that the distributions $V^{(n)}(\omega)$ and $\mathcal{T}^{(n)}(\omega)$ in the n th level $|n\rangle$ of the three-level atom depend on the atom-induced frequency shift $\mathcal{C}^{(n)}$ in Eq. (13) of the passive cavity, which indeed can distinguish which level of a three-level atom is located near the exceptional point. This means that the different levels of the three-level atom correspond to the different distributions $V^{(n)}(\omega)$ and $\mathcal{T}^{(n)}(\omega)$ in Eqs. (29) and (34), which can dispersively read out the quantum states of the three-level atom in coupled cavities with the dissipation and gain.

III. DISCUSSION CONSIDERING THE MARKOVIAN APPROXIMATION

A. Influences of the coupling strength G on the dispersive readout near the EP

To show that the perturbation to the passive cavity caused by the three-level atom can be amplified through the EP, we introduce two experimentally measurable quantities

$$\begin{aligned} \Delta E_{\pm}^1 &= \text{Re}(\Delta E_{\pm}^{(e)}) - \text{Re}(\Delta E_{\pm}^{(g)}), \\ \Delta E_{\pm}^2 &= \text{Re}(\Delta E_{\pm}^{(x)}) - \text{Re}(\Delta E_{\pm}^{(g)}), \end{aligned} \quad (35)$$

which describe the eigenfrequency differences of the system when the three-level atom is in the metastable (or excited) state and ground state, respectively, where $\Delta E_{\pm}^{(n)}$ is determined by Eq. (20). In Fig. 5 we display the eigenfrequency difference $\Delta E_{\pm}^{(j)}/\Gamma_a$ ($j = 1, 2$) versus the coupling strength G/Γ_a when the conditions $\Delta_b = 0$ and $\Gamma_a = \Gamma_b$ are satisfied. With the increase of G/Γ_a from 0 to 1, $\Delta E_{\pm}^{(j)}/\Gamma_a$ reaches a maximum at $G = G_{\text{EP}} = \Gamma_a/2$ in Eq. (22), where $\Delta E_{-}^{(j)}/\Gamma_a$ becomes the minimum, which indicates that eigenfrequency

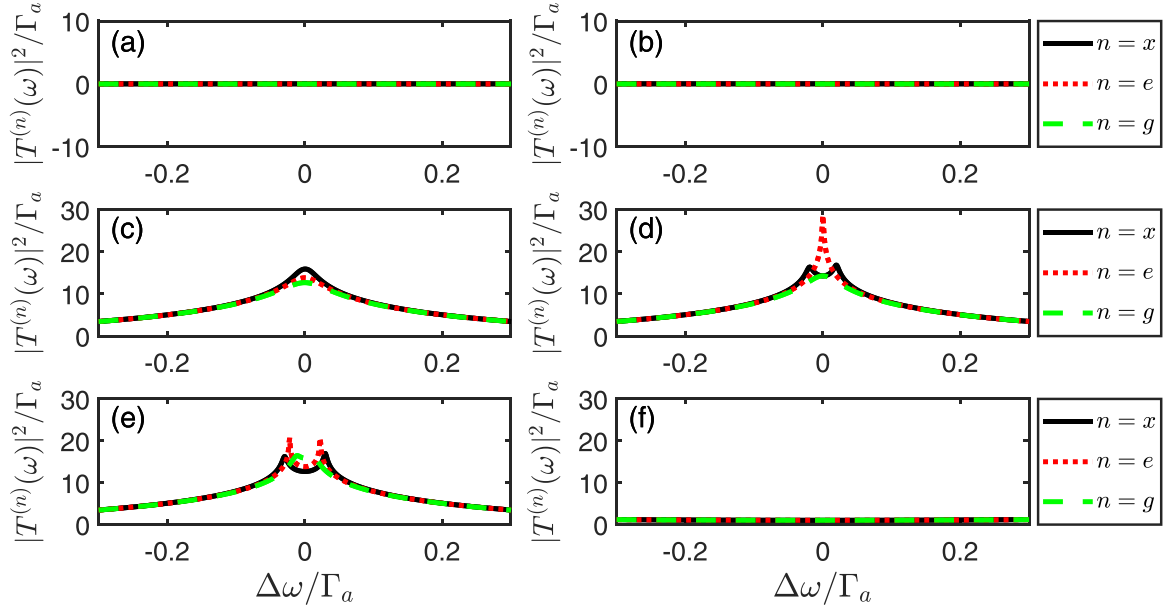


FIG. 6. Different distributions of the transmission spectrum $|T^{(n)}(\omega)|^2$ corresponding to the different levels of the three-level atom, which is calculated by Eq. (34), of the passive cavity as a function of the probe field frequency $\Delta\omega$ (the rotating frame with ω_a), for (a) $G/\Gamma_a = 0$, (b) $G/\Gamma_a = 0.0200$, (c) $G/\Gamma_a = 0.4995$, (d) $G/\Gamma_a = 0.5000$, (e) $G/\Gamma_a = 0.5005$, and (f) $G/\Gamma_a = 1.0000$. The other parameters are the same as those in Fig. 5.

differences of the system are amplified significantly near the EP in order to realize the dispersive readout of the three-level atom.

To intuitively investigate the dispersive readout, the influence of the coupling strength G on the transmission spectrum $|T^{(n)}(\omega)|^2$ is shown in Fig. 6, which varies with the probe field frequency $\Delta\omega$. In the absence of the active cavity ($G/\Gamma_a = 0$), the lines of $|T^{(n)}(\omega)|^2$ overlap when the three-level atom is in different energy levels ($n = x, e, g$) in Fig. 6(a), which makes it impossible to effectively distinguish between the quantum states of the three-level atom. It is still difficult to dispersively read out the quantum states of the atom for $G/\Gamma_a \neq 0$ but away from G_{EP}/Γ_a ($G/\Gamma_a = 0.0200, 1.0000$), as seen in Figs. 6(b) and 6(f). Fortunately, we can easily make a distinction among the three levels of the atom when the coupling strength G/Γ_a between the passive cavity and active cavity approaches the critical value $G = G_{EP}$, as found in Figs. 6(c)–6(e), which originates from the amplification of the energy spectra near the EP, where the different levels of the three-level atom correspond to the different distributions $\mathcal{T}^{(n)}(\omega)$ in Eq. (34). As a consequence, we can realize the dispersive readout of the three-level atom when the dissipation of the system is compensated by the gain of the active cavity near the EP. Next we discuss specifically the dispersive readout of the three-level atom in the absence and presence of the EP in the system.

B. Outside the EP

In this section we study the results obtained with $\Gamma_a \neq \Gamma_b$ and $G > \Gamma_a/2$, which indicates that the \mathcal{PT} symmetry of the system is not broken. In Fig. 7 we show the relationship between the eigenvalue $\Delta E_{\pm}^{(e)}$ and detuning Δ_b of the active cavity according to Eq. (20). In Fig. 7(a) the real parts of

$\Delta E_{\pm}^{(e)}$ exhibit the level repulsion, while the imaginary parts of $\Delta E_{\pm}^{(e)}$ coalesce, which implies the coupling of the passive and active cavities [128–130,137,138]. The red dashed line shows the remarkably reduced linewidth due to the coupling between passive and active cavities [129] in Fig. 7(b). In this case, the black solid line denotes the detuning Δ_b of the active cavity, whose slope changes at the regime of the coupling bandwidth.

In order to study the dispersive readout of the three-level atom more clearly, we discuss the transmission spectrum $|T^{(n)}(\omega)|^2$ of the passive cavity and the ratio of the active cavity excitation number to the input photon number $V^{(n)}(\omega)$ in Fig. 8. In Figs. 8(a) and 8(b) the lines of $|T^{(n)}(\omega)|^2$ and

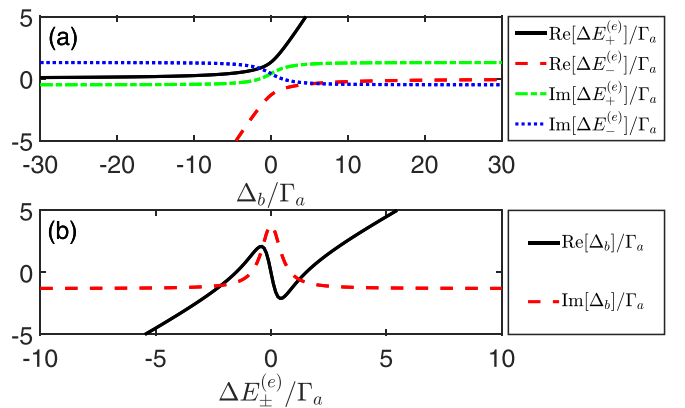


FIG. 7. (a) Real and imaginary parts of the eigenvalue $\Delta E_{\pm}^{(e)}$ determined by Eq. (20) as a function of Δ_b . (b) Real and imaginary parts of the detuning Δ_b of the active cavity [Δ_b changing with $\Delta E_{\pm}^{(e)}$ can be solved by Eq. (20)] as a function of $\Delta E_{\pm}^{(e)}$. The parameters are $G = 1.6\Gamma_a$, $\Gamma_b = 2.6\Gamma_a$, $g = 0.05\Gamma_a$, $\Omega = 0.1\Gamma_a$, $\Delta_1 = \Gamma_a$, $\Delta_2 = -2\Gamma_a$, and $\gamma_1 = \gamma_2 = 3\Gamma_a$.

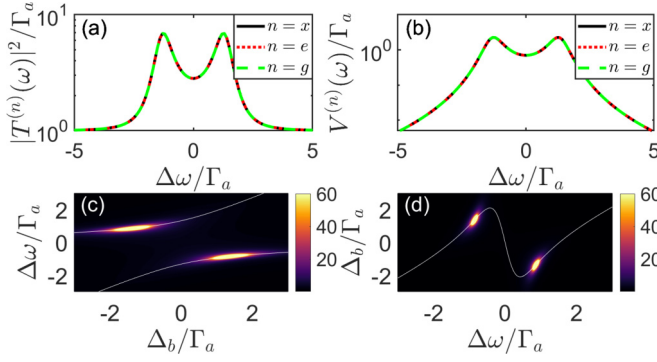


FIG. 8. (a) Transmission spectrum $|\mathcal{T}^{(n)}(\omega)|^2$ given by Eq. (34) of the passive cavity and (b) ratio of the active cavity excitation number to the input photon number $V^{(n)}(\omega)$ in Eq. (29) varying with $\Delta\omega$ without the EP. Here $|\mathcal{T}^{(e)}(\omega)|^2$ and $V^{(e)}(\omega)$ (in units of Γ_a) depend on (c) $\Delta\omega$ and (d) Δ_b without the EP. The white lines in (c) and (d) are the spectra in Figs. 7(a) and 7(b), respectively. Here $\Delta_b = 0$ and the other parameters are the same as those in Fig. 7.

$V^{(n)}(\omega)$ overlap when the EP is absent in the system, which suggests that the quantum states of the three-level atom cannot be dispersively read out. The $|\mathcal{T}^{(e)}(\omega)|^2$ and $V^{(e)}(\omega)$ varying with $\Delta\omega$ and Δ_b are shown in Figs. 8(c) and 8(d), respectively, where there are two symmetrical peaks, which confirm the system has \mathcal{PT} symmetry. The $|\mathcal{T}^{(n)}(\omega)|^2$ and $V^{(n)}(\omega)$ ($n = g, x$) present similar phenomena. The white lines passing through two peaks in Fig. 8(c) correspond to the energy spectra in Fig. 7(a), while the white line in Fig. 8(d) characterizes the detuning Δ_b of the active cavity in Fig. 7(b). It is difficult to dispersively read out the three-level atom states from the transmission coefficient and the ratio of the active cavity excitation number to the input photon number in a weak-coupling regime without the EP.

C. Dispersive readout near the EP

Compared with the case without the EP, we discuss the results satisfying $\Gamma_a = \Gamma_b$ and $G = \Gamma_a/2$, where the \mathcal{PT} -symmetry breaking leads to the existence of the EP. In Fig. 9(a) the imaginary and real parts of $\Delta E_{\pm}^{(e)}$ coalesce at $\Delta_b = 0$, i.e., $\text{Re}(\Delta E_{\pm}^{(e)}) = \text{Im}(\Delta E_{\pm}^{(e)}) = 0$, which means that the \mathcal{PT} symmetry is broken. Moreover, the imaginary part of Δ_b marked by the red dashed line becomes 0 at the resonance condition $\Delta E_{\pm}^{(e)} = 0$ due to the dissipation of the system compensated by the gain on the active cavity [132,134] in Fig. 9(b).

As shown in Fig. 10(a), the peaks of $|\mathcal{T}^{(n)}(\omega)|^2$ exhibit separation from each other when the three-level atom is in different quantum states near the EP. A similar observation for $V^{(n)}(\omega)$ is shown in Fig. 10(b), where $V^{(n)}(\omega)$ is plotted near the EP for different $\mathcal{C}^{(n)}$. In Figs. 10(a) and 10(b) we observe that the different levels of the three-level atom correspond to the different distributions $\mathcal{T}^{(n)}(\omega)$ and $V^{(n)}(\omega)$ in Eqs. (34) and (29) near the EP. It is worth noting that there is only one peak in Figs. 10(c) and 10(d), which corresponds to the position of the EP and implies that the \mathcal{PT} symmetry of the system is broken. In the same way, the white lines characterize the spectra in Figs. 9(a) and 9(b), respectively. Moreover, the

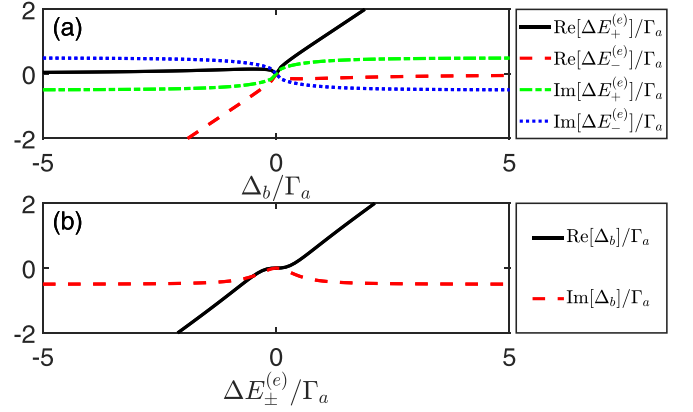


FIG. 9. (a) Real and imaginary parts of $\Delta E_{\pm}^{(e)}$ as a function Δ_b . (b) Real and imaginary parts of Δ_b as a function of $\Delta E_{\pm}^{(e)}$. Here $G = 0.5\Gamma_a$ and $\Gamma_b = \Gamma_a$ and the other parameters and vertical ordinates are the same as those in Fig. 7.

significant enhancements of $|\mathcal{T}^{(n)}(\omega)|^2$ and $V^{(n)}(\omega)$ are realized near the EP, where the perturbation differences from the passive cavity generated by the three-level atom at different energy levels are significantly amplified, which means that we can easily realize the dispersive readout of the three-level atom in the existence of the EP.

IV. NON-MARKOVIAN DISPERSIVE READOUT OF THE THREE-LEVEL ATOM

The Markovian processes successfully describe many physical phenomena, especially in the field of quantum optics, but they fail when they are applied to more complex system-environment couplings, where memory effects play dominant roles. All realistic quantum systems are open due to the unavoidable couplings to the environment [165–168]. Considering that the non-Markovian dynamics of open quantum systems is essential when the coupling between the system and environment is not weak, the characteristic times of the

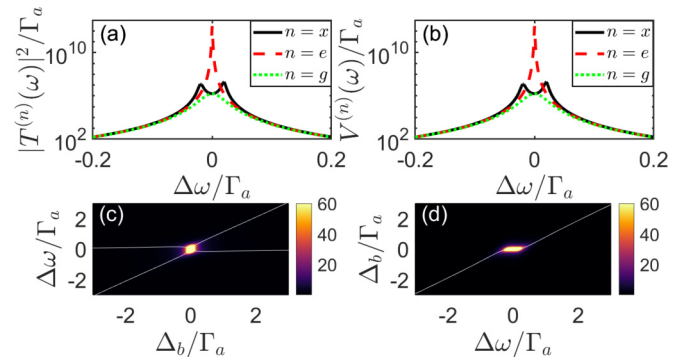


FIG. 10. Different distributions (a) $|\mathcal{T}^{(n)}(\omega)|^2$ and (b) $V^{(n)}(\omega)$ in Eqs. (34) and (29) corresponding to the different levels of the three-level atom as a function of $\Delta\omega$ near the EP. Also shown are $|\mathcal{T}^{(e)}(\omega)|^2$ and $V^{(e)}(\omega)$ (in units of Γ_a) depending on (c) $\Delta\omega$ and (d) Δ_b near the EP, where the white lines characterize the spectra in Figs. 9(a) and 9(b), respectively. Here $\Delta_b = 0$ and the other parameters and vertical ordinates are the same as those in Fig. 9.

bath are not adequately smaller than those of the system [174,185]. To realize the dispersive readout of the three-level atom weakly interacting with coupled cavities in the non-Markovian regime, the Hamiltonian (18) with the non-Markovian environment acting on the passive cavity becomes

$$\begin{aligned} \hat{H}_T = & \sum_n C^{(n)} \hat{\sigma}_{nm} \hat{a}^\dagger \hat{a} + G(\hat{a}^\dagger \hat{b} + \hat{b}^\dagger \hat{a}) + \left(\Delta_b + i \frac{\Gamma_b}{2} \right) \hat{b}^\dagger \hat{b} \\ & + \sum_k \Delta_k \hat{c}_k^\dagger \hat{c}_k + i \sum_k g_k (\hat{a}^\dagger \hat{c}_k - \hat{a} \hat{c}_k^\dagger), \end{aligned} \quad (36)$$

where $\Delta_k = \omega_k - \omega_a$, \hat{c}_k^\dagger (\hat{c}_k) is the creation (annihilation) operator of the environment with eigenfrequency ω_k , and g_k denotes the coupling strength between the passive cavity and environment. The Heisenberg-Langevin equation with Eq. (36) gives

$$\begin{aligned} \frac{d}{dt} \hat{a}(t) = & -i \sum_n C^{(n)} \hat{\sigma}_{nm} \hat{a}(t) - iG\hat{b}(t) + \sum_k g_k \hat{c}_k(t), \\ \frac{d}{dt} \hat{b}(t) = & -i \left(\Delta_b + i \frac{\Gamma_b}{2} \right) \hat{b}(t) - iG\hat{a}(t), \\ \frac{d}{dt} \hat{c}_k(t) = & -i\Delta_k \hat{c}_k(t) - g_k \hat{a}(t). \end{aligned} \quad (37)$$

The non-Markovian environmental operator is obtained by solving Eq. (37),

$$\hat{c}_k(t) = \hat{c}_k(0) e^{-i\Delta_k t} - g_k \int_0^t \hat{a}(\tau) e^{-i\Delta_k(t-\tau)} d\tau, \quad (38)$$

where the first term denotes the free propagation of the non-Markovian environment field and the second term describes the non-Markovian effects of the environment feeding back to the passive cavity. We get an integro-differential equation for the passive cavity operator by substituting Eq. (38) into Eq. (37),

$$\begin{aligned} \frac{d}{dt} \hat{a}(t) = & -i \sum_n C^{(n)} \hat{\sigma}_{nm} \hat{a}(t) - iG\hat{b}(t) + \hat{R}(t) \\ & - \int_0^t \hat{a}(\tau) f(t-\tau) d\tau, \end{aligned} \quad (39)$$

where $\hat{R}(t) = \sum_k g_k \hat{c}_k(0) e^{-i\Delta_k t} = \int_{-\infty}^{\infty} \kappa^*(t-\tau) \hat{c}_{in}(\tau) d\tau$ characterizes the coupling between the passive cavity and input field of the non-Markovian environment with the input field operator $\hat{c}_{in}(t) = \frac{1}{\sqrt{2\pi}} \sum_k \hat{c}_k(0) e^{-i\Delta_k t}$. In the continuum, the impulse response function becomes

$$\kappa(t-\tau) = \frac{1}{\sqrt{2\pi}} \int g(\omega) e^{i(\omega-\omega_a)(t-\tau)} d\omega, \quad (40)$$

where g_k is replaced by $g(\omega)$. The correlation function plays an important role in the interaction between the passive cavity and environment, which can be referred to as the memory function and is defined by

$$f(t-\tau) = \int J(\omega) e^{-i(\omega-\omega_a)t} d\omega, \quad (41)$$

where $J(\omega) = \sum_k |g_k|^2 \delta(\omega - \omega_k)$ is the spectral density of the environment. Similarly, we get

$$\hat{c}_k(t) = \hat{c}_k(t_1) e^{-i\Delta_k(t-t_1)} + g_k \int_{t_1}^t \hat{a}(\tau) e^{-i\Delta_k(t-\tau)} d\tau, \quad (42)$$

with $t \leq t_1$, and obtain

$$\begin{aligned} \frac{d}{dt} \hat{a}(t) = & -i \sum_n C^{(n)} \hat{\sigma}_{nm} \hat{a}(t) - iG\hat{b}(t) + \hat{K}(t) \\ & + \int_t^{t_1} \hat{a}(\tau) f(t-\tau) d\tau, \end{aligned} \quad (43)$$

where $\hat{K}(t) = \sum_k g_k \hat{c}_k(t_1) e^{-i\Delta_k(t-t_1)} = \int_{-\infty}^{\infty} \kappa^*(t-\tau) \hat{c}_{out}(\tau) d\tau$ with the output field operator $\hat{c}_{out}(t) = \frac{1}{\sqrt{2\pi}} \sum_k \hat{c}_k(t_1) e^{-i\Delta_k(t-t_1)}$. The non-Markovian input-output relationship is derived by comparing Eqs. (39) and (43) (setting $t_1 \rightarrow t$) [202,203],

$$\hat{c}_{out}(t) = \hat{c}_{in}(t) - \int_0^t \hat{a}(\tau) \kappa(\tau-t) d\tau, \quad (44)$$

where $\kappa(\tau-t)$ is given by Eq. (40). In the case of the Fabry-Pérot cavity [204,205], the spectral response function is defined by

$$g(\omega) = \sqrt{\frac{\Gamma_a}{2\pi}} \frac{\lambda}{\lambda - i(\omega - \omega_a)}, \quad (45)$$

where λ denotes the non-Markovian environmental spectrum width and Γ_a is the cavity dissipation through the input and output ends. The spectral density [206–208] of the environment reads

$$J(\omega) = \frac{\Gamma_a}{2\pi} \frac{\lambda^2}{\lambda^2 + (\omega - \omega_a)^2}, \quad (46)$$

which corresponds to the Lorentzian spectral density. With Eqs. (40) and (41), we obtain $\kappa(\tau-t) = \lambda \sqrt{\Gamma_a} e^{-\lambda(t-\tau)} \theta(t-\tau)$ and $f(t-\tau) = \frac{1}{2} \lambda \Gamma_a e^{-\lambda|t-\tau|}$, where $\theta(t-\tau)$ is a unit step function, $\theta(t-\tau) = 1$ for $t-\tau \geq 0$ and $\theta(t-\tau) = 0$ otherwise. In particular, the memory effect of the non-Markovian environment disappears when the spectral width λ approaches infinity. The environmental spectral density $J(\omega)$ approaches approximately $\frac{\Gamma_a}{2\pi}$ or, equivalently, the non-Markovian spectral response function $g(\omega) \rightarrow \sqrt{\frac{\Gamma_a}{2\pi}}$ in the wideband limit ($\lambda \rightarrow \infty$), which characterizes the case under the Markovian approximation. According to Eqs. (40) and (41), we have $\kappa(t) \rightarrow \sqrt{\Gamma_a} \delta(t)$ and $f(t) \rightarrow \Gamma_a \delta(t)$. Substituting the above results into Eq. (44), the Markovian input-output relation (31) can be obtained. With Eq. (39) and the second of Eqs. (37), we derive

$$\begin{aligned} \hat{A}_{NM}(\omega) = & \frac{i\tilde{\kappa}(\omega)[\hat{C}_{in}(\omega) - \hat{C}_{in}(i\lambda)]}{\hat{X} - \mathcal{Z}(\omega)}, \\ \hat{M}_{NM}(\omega) = & \frac{iG\tilde{\kappa}(\omega)[\hat{C}_{in}(\omega) - \hat{C}_{in}(i\lambda)]}{\hat{X}[\Delta\omega - \Delta_m - i(\beta - \frac{\Gamma_m}{2})] - G^2}, \end{aligned} \quad (47)$$

where $\Delta\omega = \omega - \omega_a$, $\hat{X} = \Delta\omega - \sum_n C^{(n)} \hat{\sigma}_{nm} + i f(\omega)$, $\tilde{\kappa}(\omega) = \int_{-\infty}^0 \kappa^*(t) e^{i\Delta\omega t} dt = \frac{\lambda \sqrt{\Gamma_a}}{\lambda + i\Delta\omega}$, $f(\omega) = \int_0^{\infty} f(t) e^{i\Delta\omega t}$

$dt = \frac{\lambda \Gamma_a}{2(\lambda - i\Delta\omega)}$, and $\hat{C}_{\text{in}}(\omega) = \int_0^\infty \hat{c}_{\text{in}}(t) e^{i\Delta\omega t} dt$. We obtain the spin voltage of the yttrium iron garnet (YIG) sphere in the non-Markovian regime

$$\hat{V}_{\text{NM}}(\omega) \propto \frac{\hat{\mathcal{M}}_{\text{NM}}^\dagger(\omega) \hat{\mathcal{M}}_{\text{NM}}(\omega)}{\hat{C}_{\text{in}}^\dagger(\omega) \hat{C}_{\text{in}}(\omega)} = \left| \frac{iG\tilde{\kappa}(\omega)}{\hat{X}[\Delta\omega - \Delta_m - i(\beta - \frac{\Gamma_m}{2})] - G^2} \right|^2 (1 + Q), \quad (48)$$

with

$$Q = \frac{\hat{C}_{\text{in}}^\dagger(i\lambda) \hat{C}_{\text{in}}(i\lambda) - \hat{C}_{\text{in}}^\dagger(\omega) \hat{C}_{\text{in}}(i\lambda) - \hat{C}_{\text{in}}^\dagger(i\lambda) \hat{C}_{\text{in}}(\omega)}{\hat{C}_{\text{in}}^\dagger(\omega) \hat{C}_{\text{in}}(\omega)}. \quad (49)$$

We rewrite the form of the spin voltage (48) as

$$\hat{V}_{\text{NM}}(\omega) = \sum_n V_{\text{NM}}^{(n)}(\omega) |n\rangle \langle n| (1 + Q), \quad (50)$$

with the different distributions corresponding to the different levels of the three-level atom

$$V_{\text{NM}}^{(n)}(\omega) = \left| \frac{iG\tilde{\kappa}(\omega)}{x_n[\Delta\omega - \Delta_m - i(\beta - \frac{\Gamma_m}{2})] - G^2} \right|^2, \quad (51)$$

where $x_n = \Delta\omega - \mathcal{C}^{(n)} + if(\omega)$. The term $QV_{\text{NM}}^{(n)}(\omega)$ related to $\hat{C}_{\text{in}}(i\lambda)$ in Eq. (50) is induced by the non-Markovian effects and has no Markovian counterparts, which is an inhomogeneous term depending on the specific forms of the input field $\hat{c}_{\text{in}}(t)$. Under the Markovian approximation, $QV_{\text{NM}}^{(n)}(\omega)$ tends to zero for $\lambda \rightarrow \infty$. In order to distinguish the effects of the inhomogeneous term, we assume the concrete form of the input field to be $\hat{c}_{\text{in}}(t) = c_1 e^{-\varepsilon t} \cos(h_1 t^2)$ for $\varepsilon > 0$ and $h_1 > 0$, which corresponds to $Q = \{[w_1(2x_1 - 1) - z_1(2y_1 - 1)][w_1(2x_1 - 1) - w_2(2x_2 - 1) - w_3(2x_3 - 1) - z_1(2y_1 - 1) + z_2(2y_2 - 1) + z_3(2y_3 - 1)]\} / \{[w_2(2x_2 - 1) - z_2(2y_2 - 1)][w_3(2x_3 - 1) - z_3(2y_3 - 1)]\}$, with $x_1 = fs(\frac{\varepsilon + \lambda}{\sqrt{2\pi h_1}})$, $x_2 = fs(\frac{\varepsilon - i\omega}{\sqrt{2\pi h_1}})$, $x_3 = fs(\frac{\varepsilon + i\omega}{\sqrt{2\pi h_1}})$, $y_1 = fc(\frac{\varepsilon + \lambda}{\sqrt{2\pi h_1}})$, $y_2 = fc(\frac{\varepsilon - i\omega}{\sqrt{2\pi h_1}})$, $y_3 = fc(\frac{\varepsilon + i\omega}{\sqrt{2\pi h_1}})$, $z_1 = \sin(\frac{(\varepsilon + \lambda)^2}{4h_1})$, $z_2 = \sin(\frac{(\varepsilon - i\omega)^2}{4h_1})$, $z_3 = \sin(\frac{(\varepsilon + i\omega)^2}{4h_1})$, $w_1 = \cos(\frac{(\varepsilon + \lambda)^2}{4h_1})$, $w_2 = \cos(\frac{(\varepsilon - i\omega)^2}{4h_1})$, and $w_3 = \cos(\frac{(\varepsilon + i\omega)^2}{4h_1})$, where $fs(z) = \int_0^z \sin(\pi t^2/2) dt$ and $fc(z) = \int_0^z \cos(\pi t^2/2) dt$. We show that the inhomogeneous term cannot reveal the characteristics of the system under probe. For the concrete input field and given parameters, e.g., $\varepsilon = 0.0001\Gamma_a$ and $h_1 = 0.0001\Gamma_a$, we can evaluate $Q \sim 10^{-2}$ for $\lambda = 0.6\Gamma_a$ (non-Markovian regime) and $Q \sim 10^{-4}$ for $\lambda = 40\Gamma_a$ (weak non-Markovian effect) when ω approaches ω_a . The inhomogeneous term $QV_{\text{NM}}^{(n)}(\omega)$ is much smaller than $V_{\text{NM}}^{(n)}(\omega)$, which can be ignored for these parameters and leads to $\hat{V}_{\text{NM}}(\omega) \sim V_{\text{NM}}^{(n)}(\omega)$ for some special forms of input fields. Therefore, the influence of the inhomogeneous term on the ratio of the active cavity excitation number to the input photon number is not considered in subsequent plots.

Moreover, we get the transmission coefficient $\hat{\mathcal{T}}_{\text{NM}}(\omega)$ by making the modified Laplace transformation to the

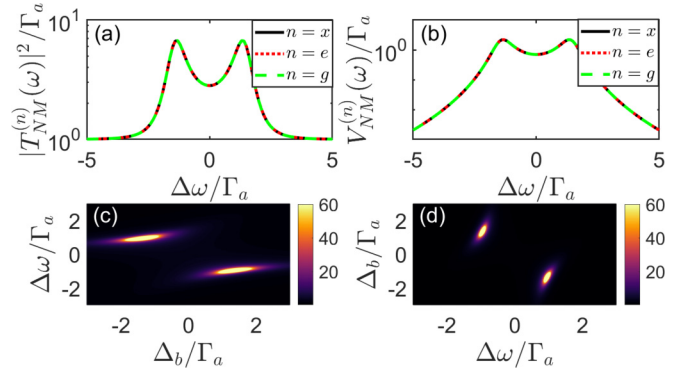


FIG. 11. Plots of (a) $|\mathcal{T}_{\text{NM}}^{(n)}(\omega)|^2$ calculated by Eq. (53) and (b) $V_{\text{NM}}^{(n)}(\omega)$ in Eq. (51) as a function of $\Delta\omega$ without the EP in the non-Markovian regime with $\lambda = 4\Gamma_a$. Also shown are $|\mathcal{T}_{\text{NM}}^{(n)}(\omega)|^2$ and $V_{\text{NM}}^{(n)}(\omega)$ (in units of Γ_a) depending on (c) $\Delta\omega$ and (d) Δ_b without the EP in the non-Markovian regime with $\lambda = 4\Gamma_a$. The other parameters are the same as those in Fig. 8.

non-Markovian input-output relationship (44),

$$\hat{\mathcal{T}}_{\text{NM}}(\omega) = 1 - \frac{i\kappa(-\omega)\tilde{\kappa}(\omega)}{\Delta\omega - \sum_n \mathcal{C}^{(n)}\delta_{nm} + if(\omega) - \mathcal{Z}(\omega)} + \frac{i\kappa(-\omega)\tilde{\kappa}(\omega)\hat{C}_{\text{in}}(i\lambda)/\hat{C}_{\text{in}}(\omega)}{\Delta\omega - \sum_n \mathcal{C}^{(n)}\delta_{nm} + if(\omega) - \mathcal{Z}(\omega)}, \quad (52)$$

where $\kappa(-\omega) = \int_0^\infty \kappa(-t) e^{i\Delta\omega t} dt = \frac{\lambda\sqrt{\Gamma_a}}{\lambda - i\Delta\omega}$. For the concrete input field $\hat{c}_{\text{in}}(t) = c_1 e^{-\varepsilon t} \cos(h_1 t^2)$ with $\varepsilon > 0$ and $h_1 > 0$, we obtain $\hat{C}_{\text{in}}(i\lambda)/\hat{C}_{\text{in}}(\omega) = [w_1(2x_1 - 1) - z_1(2y_1 - 1)] / [w_2(2x_2 - 1) - z_2(2y_2 - 1)]$, which leads to $\hat{C}_{\text{in}}(i\lambda)/\hat{C}_{\text{in}}(\omega) \sim 10^{-2}$ for $\lambda = 0.6\Gamma_a$ and $\hat{C}_{\text{in}}(i\lambda)/\hat{C}_{\text{in}}(\omega) \sim 10^{-4}$ for $\lambda = 40\Gamma_a$. Similar to Eq. (50), the third term in Eq. (52) is an inhomogeneous term induced by the non-Markovian effects, which can be neglected. Therefore, we can consider only the first two terms of Eq. (52), which results in $\hat{\mathcal{T}}_{\text{NM}}(\omega) = \sum_n \mathcal{T}_{\text{NM}}^{(n)}(\omega) |n\rangle \langle n|$, with the different distributions corresponding to the different levels of the three-level atom

$$\mathcal{T}_{\text{NM}}^{(n)}(\omega) = 1 - \frac{i\kappa(-\omega)\tilde{\kappa}(\omega)}{\Delta\omega - \mathcal{C}^{(n)} + if(\omega) - \mathcal{Z}(\omega)}. \quad (53)$$

In the non-Markovian limit, i.e., $\lambda \rightarrow \infty$, we have $\kappa(-\omega) \rightarrow \sqrt{\Gamma_a}$, $\tilde{\kappa}(\omega) \rightarrow \sqrt{\Gamma_a}$, and $f(\omega) \rightarrow \frac{\Gamma_a}{2}$, which make the results given by Eqs. (51) and (53) able to return to those obtained under the Markovian approximation defined by Eqs. (29) and (34).

V. INFLUENCE OF NON-MARKOVIAN EFFECTS ON DISPERSIVE READOUT

In this section we discuss the dispersive readout for the three-level system weakly interacting with coupled cavities without an EP in the non-Markovian regime. The $|\mathcal{T}_{\text{NM}}^{(n)}(\omega)|^2$ calculated by Eq. (53) and $V_{\text{NM}}^{(n)}(\omega)$ in Eq. (51) as a function of $\Delta\omega$ are shown in Figs. 11(a) and 11(b), respectively, where the quantum states of the three-level atom cannot be distinguished due to the overlap of the lines. In Figs. 11(c) and 11(d) the two symmetric peaks appear, which leads to a conclusion similar

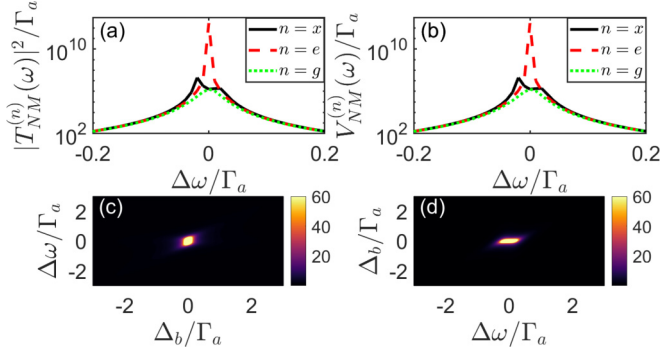


FIG. 12. Different distributions (a) $|\mathcal{T}_{NM}^{(n)}(\omega)|^2$ and (b) $V_{NM}^{(n)}(\omega)$ in Eqs. (53) and (51), corresponding to the different levels of the three-level atom near the EP, plotted to realize the dispersive readout in the non-Markovian regime with $\lambda = 4\Gamma_a$. Also shown are $|\mathcal{T}_{NM}^{(e)}(\omega)|^2$ and $V_{NM}^{(e)}(\omega)$ (in units of Γ_a) as a function of (c) $\Delta\omega$ and (d) Δ_b near the EP in the non-Markovian regime for $\lambda = 4\Gamma_a$. The other parameters are the same as those in Fig. 10.

to the Markovian case that the states of the three-level atom are difficult to dispersively read out when the \mathcal{PT} symmetry of the system still exists. However, we can realize the dispersive readout when the \mathcal{PT} symmetry is broken, which means the system is near the EP between the \mathcal{PT} -symmetric and \mathcal{PT} -symmetry-broken regimes in Figs. 12(a) and 12(b), where the different levels of the three-level atom correspond to the different distributions $|\mathcal{T}_{NM}^{(n)}(\omega)|^2$ and $V_{NM}^{(n)}(\omega)$ in Eqs. (53) and (51). Figure 12(c) shows the only peak of $|\mathcal{T}_{NM}^{(e)}(\omega)|^2$ varying with $\Delta\omega$ and Δ_b , which implies the \mathcal{PT} symmetry of the system is broken. A similar observation is made for $V_{NM}^{(e)}(\omega)$ in Fig. 12(d), which points out that the dispersive readout of the three-level atom can be realized near the EP.

We specifically study the influence of the non-Markovian environment spectral width λ on the dispersive readout for three-level atom near the EP. First, we consider $|\mathcal{T}_{NM}^{(n)}(\omega)|^2$ and $V_{NM}^{(n)}(\omega)$ varying with $\Delta\omega$ when the spectral width λ is very small in Figs. 13 and 14, respectively. As the spectral width λ

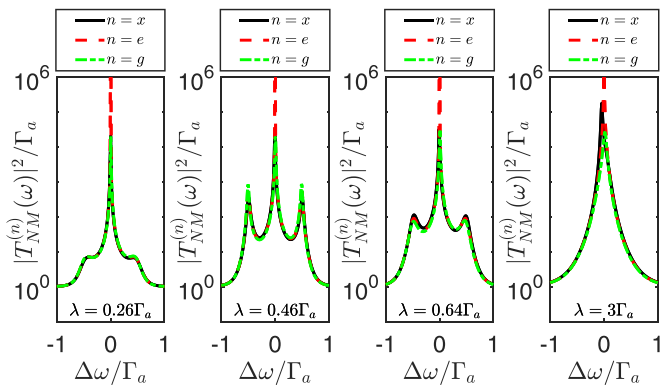


FIG. 13. Different distributions $|\mathcal{T}_{NM}^{(n)}(\omega)|^2$ corresponding to the different levels of the three-level atom as a function of $\Delta\omega$ near the EP are solved by Eq. (53) in the non-Markovian regime, where the environmental spectrum width λ varies from $0.26\Gamma_a$ to $3\Gamma_a$. The parameters are $\Delta_b = 0$, $G = 0.5\Gamma_a$, $\Gamma_b = \Gamma_a$, $g = 0.05\Gamma_a$, $\Omega = 0.1\Gamma_a$, $\Delta_1 = \Gamma_a$, $\Delta_2 = -2\Gamma_a$, and $\gamma_1 = \gamma_2 = 3\Gamma_a$.

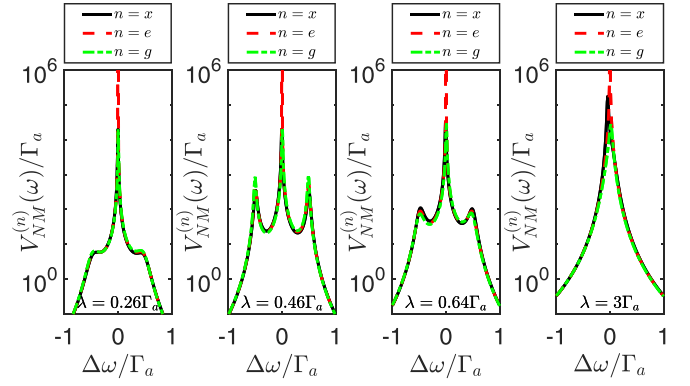


FIG. 14. Different distributions $V_{NM}^{(n)}(\omega)$ given by Eq. (51) corresponding to the different levels of the three-level atom versus $\Delta\omega$ near the EP shown in the non-Markovian regime. The parameters chosen the same as those in Fig. 13.

increases from $0.26\Gamma_a$ to $3\Gamma_a$, the distributions $|\mathcal{T}_{NM}^{(n)}(\omega)|^2$ and $V_{NM}^{(n)}(\omega)$ are obviously different when the three-level atom is in the level $|e\rangle$ compared with the case of the other two levels, i.e., $|x\rangle$ and $|g\rangle$. In other words, it is convenient to dispersively read out the metastable state $|e\rangle$ of the three-level atom by adjusting the spectral width λ when the non-Markovian effects become strong, which originates from the strong excitation backflow obtained by the interaction between the system and environment.

With the increase of the spectral width λ varying from $8\Gamma_a$ to $400\Gamma_a$, the relative heights of the two peaks undergo a significant change, where the left peak of the double peak gradually transfers to the right peak when the atom is in the excited state $|x\rangle$, as seen in Fig. 15, while the lines in the case of the ground state $|g\rangle$ and metastable state $|e\rangle$ overlap for the different spectral widths in Figs. 16 and 17, respectively. The similar observation in Fig. 18 for $V_{NM}^{(x)}(\omega)$ can be explained by the excitation backflow originating from the non-Markovian effects of the environment. This indicates that the feedback effect of the non-Markovian environment acting on the system dynamics can enhance the dispersive readout for the excited

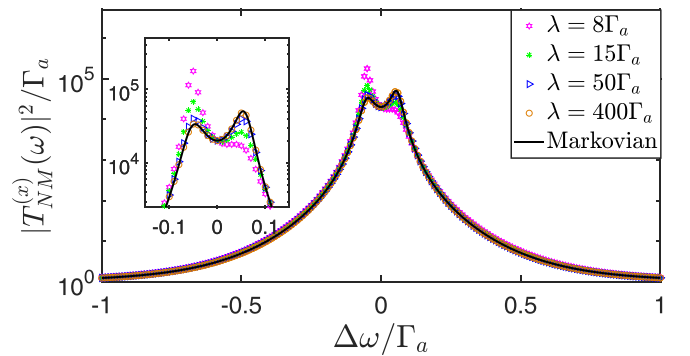


FIG. 15. Plot of $|\mathcal{T}_{NM}^{(x)}(\omega)|^2$, determined by Eq. (53), as a function of $\Delta\omega$ near the EP in the non-Markovian regime, where the spectral width λ increases from $8\Gamma_a$ to $400\Gamma_a$. The non-Markovian dispersive readout is consistent with that obtained by the Markovian approximation in the wideband limit ($\lambda \rightarrow \infty$). The other parameters are the same as those in Fig. 13.

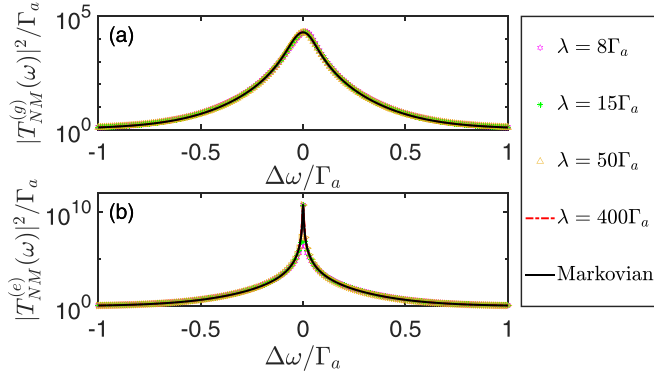


FIG. 16. Plot of (a) $|\mathcal{T}_{NM}^{(g)}(\omega)|^2$ and (b) $|\mathcal{T}_{NM}^{(e)}(\omega)|^2$ versus $\Delta\omega$ near the EP in the non-Markovian regime. The parameters are the same as those in Fig. 15.

state $|x\rangle$ in the three-level atom. In particular, $|\mathcal{T}_{NM}^{(x)}(\omega)|^2$ and $V_{NM}^{(x)}(\omega)$ in the non-Markovian case are highly consistent with those under the Markovian approximation ($\lambda \rightarrow \infty$) when the spectral width λ is large enough ($\lambda = 400\Gamma_a$). In this case, the impulse response function (40) and correlation function (41) tend to $\sqrt{\Gamma_a}\delta(t)$ and $\Gamma_a\delta(t)$, respectively, in the wideband limit, i.e., the detuning width λ approaches infinity, which leads to Eqs. (39) and (44) with the non-Markovian limit returning to Eqs. (23) and (31) under the Markovian approximation. Therefore, we can achieve enhancement of the dispersive readout for any interaction strength λ in the non-Markovian environment by adjusting the model parameters of the system.

VI. CONCLUSION

In summary, we have studied the dispersive readout of the driven three-level atom weakly interacting with a passive cavity that couples to an active cavity. The conditions for the existence of the \mathcal{PT} -symmetric phase transition in the quantum system were derived by examining the eigenvalues of the effective Hamiltonian, which reflects that the perturbation to the passive cavity caused by the three-level atom can be prominently amplified near the EP. We realized the dispersive readout of the excited, metastable, and ground states for the

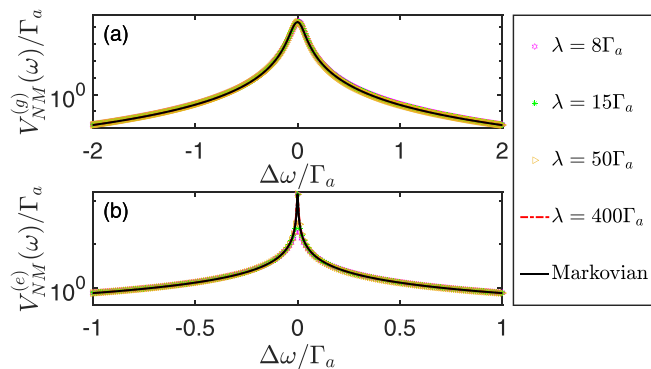


FIG. 17. Plot of $V_{NM}^{(n)}(\omega)$ ($n = g, e$) calculated by Eq. (51) as a function of $\Delta\omega$ near the EP in the non-Markovian regime. The parameters are the same as those in Fig. 15.

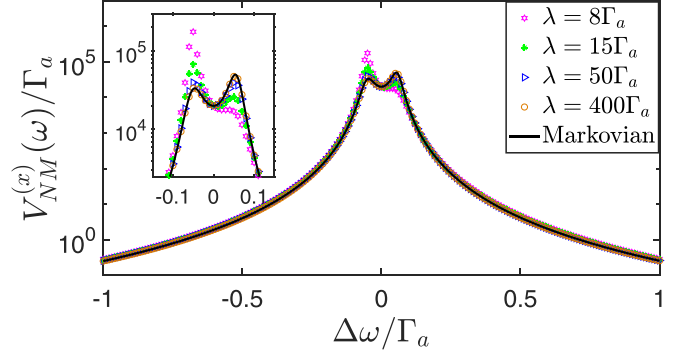


FIG. 18. Plot of $V_{NM}^{(x)}(\omega)$ as a function of $\Delta\omega$ near the EP in the non-Markovian regime. As the spectral width λ increases, the non-Markovian dispersive readout gradually tends to the case of the Markovian approximation ($\lambda \rightarrow \infty$). The parameters are the same as those in Fig. 15.

three-level atom in the weak-coupling regime via comparing the different characteristics of the transmission spectrum of the passive cavity and the ratio of the active cavity excitation number to the input photon number obtained by using the modified Laplace transform and input-output theory whether the EP exists in the system or not. Compared with the dispersive readout method in the strong-coupling regime, the proposed dispersive readout scheme involves only the weak-coupling regime, which can suppress unwanted backaction [5,6] of the dispersive readout on the three-level atom.

Moreover, we have extended the dispersive readout of the three-level atom to the non-Markovian regime, where the results obtained under the Markovian approximation were found to be consistent with those in the non-Markovian regime in the wideband limit. The environmental spectral width in the non-Markovian regime can effectively enhance the dispersive readout of the three-level atom due to the excitation backflow induced by the coupling between the passive cavity and environment. The dispersive readout proposed can deepen the understanding of the relationship between \mathcal{PT} symmetry plus non-Markovian effects and dispersive readout.

As an outlook, it would be interesting to investigate the total excitation number of nonconserving systems beyond the rotating-wave approximation, e.g., the non-rotating-wave interaction between the passive cavity and environment $\sum_k J_k(\hat{a} + \hat{a}^\dagger)(\hat{c}_k + \hat{c}_k^\dagger)$ [122,209,210], anisotropic non-rotating-wave interaction $\sum_k \zeta_k(\hat{c}_k\hat{a}^\dagger + \hat{c}_k^\dagger\hat{a}) + \xi_k(\hat{c}_k\hat{a} + \hat{c}_k^\dagger\hat{a}^\dagger)$ [211–217], and many-body models [218–223]. More generally, the total systems containing the external environment beyond the RWA deserve future explorations that are not limited to the cases of the anisotropic non-rotating-wave approximation, i.e., all the couplings between different subsystems might be of the form $\sum_{n,k} (G_{n,k}\hat{Y}_n\hat{Z}_k^\dagger + G_{n,k}^*\hat{Y}_n^\dagger\hat{Z}_k + J_{n,k}\hat{Y}_n\hat{Z}_k + J_{n,k}^*\hat{Y}_n^\dagger\hat{Z}_k^\dagger)$, where \hat{Y}_n^\dagger (\hat{Y}_n) and \hat{Z}_k^\dagger (\hat{Z}_k) are the creation (annihilation) operators for the total systems (including the three-level atom, coupled cavities, the classical driving field, and the environment), while $G_{n,k}$ and $J_{n,k}$ denote the coupling strengths of the rotating-wave and non-rotating-wave interactions, respectively.

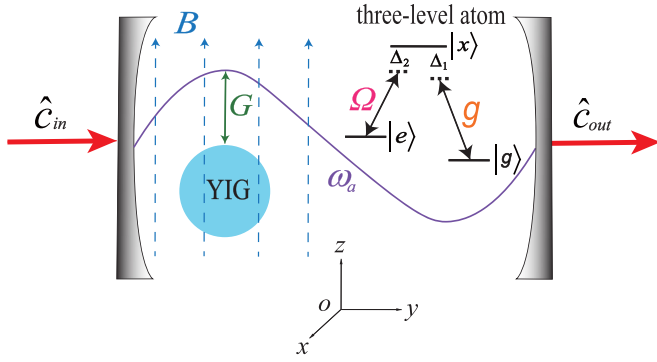


FIG. 19. The dispersive readout of the driven three-level atom might also be realized in the cavity-magnon system [128–130]. The atom weakly interacting with the cavity (eigenfrequency ω_a) with the coupling strength g has three relevant electronic levels, i.e., the excited state $|x\rangle$, metastable state $|e\rangle$, and ground state $|g\rangle$. The transition from level $|e\rangle$ to level $|x\rangle$ is driven by the classical driving field with strength Ω and frequency ω_l . The YIG sphere coupled to the cavity with the coupling strength G is located at the maximum magnetic field of the cavity perpendicular to the uniform bias magnetic field with strength B in the direction of the z axis. The \hat{c}_{in} and \hat{c}_{out} denote the input-field and output-field operators, respectively. The cavity and the classical driving field are detuned from the three-level atom and are denoted by Δ_1 and Δ_2 , respectively.

ACKNOWLEDGMENTS

This work was supported by National Natural Science Foundation of China under Grant No. 12274064, Scientific Research Project for Department of Education of Jilin Province under Grant No. JJKH20241410KJ, and Natural Science Foundation of Jilin Province (subject arrangement project) under Grant No. 20210101406JC.

APPENDIX A: WEAK COUPLING OF A CAVITY-MAGNON SYSTEM TO A DRIVEN THREE-LEVEL ATOM

The system in our scheme might also consist of a driven three-level atom weakly coupled to the cavity, which interacts

with the YIG sphere by the strong-coupling strength G due to the characteristics of the YIG sphere in Fig. 19. A uniform bias magnetic field in the direction of the z axis is exerted on the YIG sphere situated at the maximum magnetic field of the cavity mode, which is perpendicular to the bias magnetic field [224–243]. In order to ignore the Heisenberg exchange effects, we choose the YIG sphere of the paramagnetic material [244].

When the dissipation of the system can be compensated exactly by the gain from the torque [134,245–247] exerted on the YIG sphere, the real and imaginary parts of the eigenvalues coalesce at the EP [the condition of the \mathcal{PT} -symmetric phase transition is similar to Eq. (22)] by varying the torque. The sensitivity of dispersive readout can be enhanced near the EP [248–250], which contributes to the dispersive readout of the excited, metastable, and ground states of the three-level atom via the transmission of the cavity [251–254] and spin voltage of the YIG sphere [255].

APPENDIX B: DERIVATION OF EQ. (22)

The exceptional point corresponding to two eigenenergies and their eigenstates coalescing, i.e., $4G^2 + (\Delta_b + i\Gamma_a/2 + i\Gamma_b/2)^2 = 0$ in Eq. (20), gives $4G^2 + (\Delta_b + i\eta)^2 = 0$ with $\eta = \Gamma_a/2 + \Gamma_b/2$ (when we study the exceptional point, the atom is not considered, i.e., $C^{(n)} = 0$) or $4G^2 + \Delta_b^2 + 2\Delta_b\eta i - \eta^2 = 0$, which leads to

$$\Delta_b\eta = 0, \quad (\text{B1})$$

$$4G^2 + \Delta_b^2 - \eta^2 = 0. \quad (\text{B2})$$

With Eqs. (B1) and (B2), two possible cases should be considered. (i) In the first case, we assume $\Delta_b = 0$ for Eq. (B1), which results in $G = \eta/2$. For the balanced dissipation and gain from passive and active cavities, i.e., $\Gamma_a = \Gamma_b$, we have $G = \Gamma_a/2$ and obtain Eq. (22). (ii) For $\Delta_b \neq 0$ and $\eta = 0$, we arrive at $G = 0$ and $\Delta_b = 0$ from Eq. (B2), which is not consistent with the assumption $\Delta_b \neq 0$ and should be discarded.

- [1] M. A. Nielsen and I. L. Chuang, *Quantum Computation and Quantum Information* (Cambridge University Press, Cambridge, 2000).
- [2] C. H. Bennett and D. P. DiVincenzo, Quantum information and computation, *Nature (London)* **404**, 247 (2000).
- [3] A. Steane, Quantum computing, *Rep. Prog. Phys.* **61**, 117 (1998).
- [4] A. Blais, R. S. Huang, A. Wallraff, S. M. Girvin, and R. J. Schoelkopf, Cavity quantum electrodynamics for superconducting electrical circuits: An architecture for quantum computation, *Phys. Rev. A* **69**, 062320 (2004).
- [5] A. Wallraff, D. I. Schuster, A. Blais, L. Frunzio, R. S. Huang, J. Majer, S. Kumar, S. M. Girvin, and R. J. Schoelkopf, Strong coupling of a single photon to a superconducting qubit using circuit quantum electrodynamics, *Nature (London)* **431**, 162 (2004).
- [6] J. Gambetta, A. Blais, D. I. Schuster, A. Wallraff, L. Frunzio, J. Majer, M. H. Devoret, S. M. Girvin, and R. J. Schoelkopf,

Qubit-photon interactions in a cavity: Measurement-induced dephasing and number splitting, *Phys. Rev. A* **74**, 042318 (2006).

- [7] A. Blais, J. Gambetta, A. Wallraff, D. I. Schuster, S. M. Girvin, M. H. Devoret, and R. J. Schoelkopf, Quantum-information processing with circuit quantum electrodynamics, *Phys. Rev. A* **75**, 032329 (2007).
- [8] Z. L. Xiang, S. Ashhab, J. Q. You, and F. Nori, Hybrid quantum circuits: Superconducting circuits interacting with other quantum systems, *Rev. Mod. Phys.* **85**, 623 (2013).
- [9] G. Kurizki, P. Bertet, Y. Kubo, K. Mølmer, D. Petrosyan, P. Rabl, and J. Schmiedmayer, Quantum technologies with hybrid systems, *Proc. Natl. Acad. Sci. USA* **112**, 3866 (2015).
- [10] R. J. Schoelkopf and S. M. Girvin, Wiring up quantum systems, *Nature (London)* **451**, 664 (2008).
- [11] G. Johansson, L. Tornberg, V. S. Shumeiko, and G. Wendin, Readout methods and devices for Josephson-junction-based solid-state qubits, *J. Phys.: Condens. Matter* **18**, S901 (2006).

- [12] G. Johansson, L. Tornberg, and C. M. Wilson, Fast quantum limited readout of a superconducting qubit using a slow oscillator, *Phys. Rev. B* **74**, 100504(R) (2006).
- [13] D. I. Schuster, A. A. Houck, J. A. Schreier, A. Wallraff, J. M. Gambetta, A. Blais, L. Frunzio, J. Majer, B. Johnson, M. H. Devoret, S. M. Girvin, and R. J. Schoelkopf, Resolving photon number states in a superconducting circuit, *Nature (London)* **445**, 515 (2007).
- [14] R. Bianchetti, S. Filipp, M. Baur, J. M. Fink, M. Göppl, P. J. Leek, L. Steffen, A. Blais, and A. Wallraff, Dynamics of dispersive single-qubit readout in circuit quantum electrodynamics, *Phys. Rev. A* **80**, 043840 (2009).
- [15] T. Wirth, J. Lisenfeld, A. Lukashenko, and A. V. Ustinov, Microwave readout scheme for a Josephson phase qubit, *Appl. Phys. Lett.* **97**, 262508 (2010).
- [16] G. Q. Zhang, Y. P. Wang, and J. Q. You, Dispersive readout of a weakly coupled qubit via the parity-time-symmetric phase transition, *Phys. Rev. A* **99**, 052341 (2019).
- [17] D. I. Schuster, Circuit quantum electrodynamics, Ph.D. thesis, Yale University, 2007.
- [18] T. Lin, S. S. Gu, Y. Q. Xu, S. L. Jiang, N. Wang, B. C. Wang, H. O. Li, G. Cao, and G. P. Guo, Circuit-QED based time-averaged dispersive readout of a semiconductor charge qubit, *Appl. Phys. Lett.* **121**, 184004 (2022).
- [19] S. Park, C. Metzger, L. Tosi, M. F. Goffman, C. Urbina, H. Pothier, and A. L. Yeyati, From adiabatic to dispersive readout of quantum circuits, *Phys. Rev. Lett.* **125**, 077701 (2020).
- [20] M. Mergenthaler, A. Nersisyan, A. Patterson, M. Esposito, A. Baumgartner, C. Schönenberger, G. A. D. Briggs, E. A. Laird, and P. J. Leek, Circuit quantum electrodynamics with carbon-nanotube-based superconducting quantum circuits, *Phys. Rev. Appl.* **15**, 064050 (2021).
- [21] A. Blais, A. L. Grimsmo, S. M. Girvin, and A. Wallraff, Circuit quantum electrodynamics, *Rev. Mod. Phys.* **93**, 025005 (2021).
- [22] K. N. Nesterov, I. V. Pechenezhskiy, and M. G. Vavilov, Counting statistics of microwave photons in circuit QED, *Phys. Rev. A* **101**, 052321 (2020).
- [23] P. Scarlino, D. J. van Woerkom, A. Stockklauser, J. V. Koski, M. C. Collodo, S. Gasparinetti, C. Reichl, W. Wegscheider, T. Ihn, K. Ensslin, and A. Wallraff, All-microwave control and dispersive readout of gate-defined quantum dot qubits in circuit quantum electrodynamics, *Phys. Rev. Lett.* **122**, 206802 (2019).
- [24] W. Feng, C. Zhang, Z. Wang, L. P. Qin, and X. Q. Li, Gradual partial-collapse theory for ideal nondemolition longitudinal readout of qubits in circuit QED, *Phys. Rev. A* **98**, 022121 (2018).
- [25] M. Schöndorf and F. K. Wilhelm, Nonlinear parity readout with a microwave photodetector, *Phys. Rev. A* **97**, 043849 (2018).
- [26] N. Lambert, M. Cirio, M. Delbecq, G. Allison, M. Marx, S. Tarucha, and F. Nori, Amplified and tunable transverse and longitudinal spin-photon coupling in hybrid circuit-QED, *Phys. Rev. B* **97**, 125429 (2018).
- [27] C. C. Bultink, M. A. Rol, T. E. O'Brien, X. Fu, B. C. S. Dikken, C. Dickel, R. F. L. Vermeulen, J. C. de Sterke, A. Bruno, R. N. Schouten, and L. DiCarlo, Active resonator reset in the nonlinear dispersive regime of circuit QED, *Phys. Rev. Appl.* **6**, 034008 (2016).
- [28] J. L. Orgiazzi, C. Deng, D. Layden, R. Marchildon, F. Kitapli, F. Shen, M. Bal, F. R. Ong, and A. Lupascu, Flux qubits in a planar circuit quantum electrodynamics architecture: Quantum control and decoherence, *Phys. Rev. B* **93**, 104518 (2016).
- [29] G. Y. Zhu, D. G. Ferguson, V. E. Manucharyan, and J. Koch, Circuit QED with fluxonium qubits: Theory of the dispersive regime, *Phys. Rev. B* **87**, 024510 (2013).
- [30] A. P. Sears, A. Petrenko, G. Catelani, L. Sun, H. Paik, G. Kirchmair, L. Frunzio, L. I. Glazman, S. M. Girvin, and R. J. Schoelkopf, Photon shot noise dephasing in the strong-dispersive limit of circuit QED, *Phys. Rev. B* **86**, 180504(R) (2012).
- [31] M. R. Delbecq, V. Schmitt, F. D. Parmentier, N. Roch, J. J. Viennot, G. Fève, B. Huard, C. Mora, A. Cottet, and T. Kontos, Coupling a quantum dot, fermionic leads, and a microwave cavity on a chip, *Phys. Rev. Lett.* **107**, 256804 (2011).
- [32] W. Feng, P. Y. Wang, X. M. Ding, L. T. Xu, and X. Q. Li, Generating and stabilizing the Greenberger-Horne-Zeilinger state in circuit QED: Joint measurement, Zeno effect, and feedback, *Phys. Rev. A* **83**, 042313 (2011).
- [33] L. Tornberg and G. Johansson, High-fidelity feedback-assisted parity measurement in circuit QED, *Phys. Rev. A* **82**, 012329 (2010).
- [34] K. Lalumière, J. M. Gambetta, and A. Blais, Tunable joint measurements in the dispersive regime of cavity QED, *Phys. Rev. A* **81**, 040301(R) (2010).
- [35] M. Boissonneault, J. M. Gambetta, and A. Blais, Dispersive regime of circuit QED: Photon-dependent qubit dephasing and relaxation rates, *Phys. Rev. A* **79**, 013819 (2009).
- [36] S. Kumar and D. P. DiVincenzo, Exploiting Kerr cross nonlinearity in circuit quantum electrodynamics for nondemolition measurements, *Phys. Rev. B* **82**, 014512 (2010).
- [37] C. C. Bultink, B. Tarasinski, N. Haandbæk, S. Poletto, N. Haider, D. J. Michalak, A. Bruno, and L. DiCarlo, General method for extracting the quantum efficiency of dispersive qubit readout in circuit QED, *Appl. Phys. Lett.* **112**, 092601 (2018).
- [38] P. Huembeli and S. E. Nigg, Towards a heralded eigenstate-preserving measurement of multi-qubit parity in circuit QED, *Phys. Rev. A* **96**, 012313 (2017).
- [39] D. H. Slichter, R. Vijay, S. J. Weber, S. Boutin, M. Boissonneault, J. M. Gambetta, A. Blais, and I. Siddiqi, Measurement-induced qubit state mixing in circuit QED from up-converted dephasing noise, *Phys. Rev. Lett.* **109**, 153601 (2012).
- [40] A. Crippa, R. Ezzouch, A. Aprá, A. Amisse, R. Laviéville, L. Hutin, B. Bertrand, M. Vinet, M. Urdampilleta, T. Meunier, M. Sanquer, X. Jehl, R. Maurand, and S. De Franceschi, Gate-reflectometry dispersive readout and coherent control of a spin qubit in silicon, *Nat. Commun.* **10**, 2776 (2019).
- [41] K. D. Petersson, L. W. McFaul, M. D. Schroer, M. Jung, J. M. Taylor, A. A. Houck, and J. R. Petta, Circuit quantum electrodynamics with a spin qubit, *Nature (London)* **490**, 380 (2012).
- [42] T. Frey, P. J. Leek, M. Beck, A. Blais, T. Ihn, K. Ensslin, and A. Wallraff, Dipole coupling of a double quantum dot to a microwave resonator, *Phys. Rev. Lett.* **108**, 046807 (2012).
- [43] R. Ezzouch, S. Zihlmann, V. P. Michal, J. Li, A. Aprá, B. Bertrand, L. Hutin, M. Vinet, M. Urdampilleta, T. Meunier, X. Jehl, Y. M. Niquet, M. Sanquer, S. De Franceschi, and

- R. Maurand, Dispersively probed microwave spectroscopy of a silicon hole double quantum dot, *Phys. Rev. Appl.* **16**, 034031 (2021).
- [44] D. de Jong, C. G. Prosko, D. M. A. Waardenburg, L. Han, F. K. Malinowski, P. Krogstrup, L. P. Kouwenhoven, J. V. Koski, and W. Pfaff, Rapid microwave-only characterization and readout of quantum dots using multiplexed gigahertz-frequency resonators, *Phys. Rev. Appl.* **16**, 014007 (2021).
- [45] T. Lundberg, J. Li, L. Hutin, B. Bertrand, D. J. Ibberson, C. M. Lee, D. J. Niegemann, M. Urdampilleta, N. Stelmashenko, T. Meunier, J. W. A. Robinson, L. Ibberson, M. Vinet, Y. M. Niquet, and M. F. Gonzalez-Zalba, Spin quintet in a silicon double quantum dot: Spin blockade and relaxation, *Phys. Rev. X* **10**, 041010 (2020).
- [46] R. Ruskov and C. Tahan, Quantum-limited measurement of spin qubits via curvature couplings to a cavity, *Phys. Rev. B* **99**, 245306 (2019).
- [47] J. Duan, J. S. Lehtinen, M. A. Fogarty, S. Schaal, M. M. L. Lam, A. Ronzani, A. Shchepetov, P. Koppinen, M. Prunnila, F. Gonzalez-Zalba, and J. J. L. Morton, Dispersive readout of reconfigurable ambipolar quantum dots in a silicon-on-insulator nanowire, *Appl. Phys. Lett.* **118**, 164002 (2021).
- [48] A. R. Schmidt, E. Henry, C. C. Lo, Y. T. Wang, H. Li, L. Greenman, O. Namaan, T. Schenkel, K. B. Whaley, J. Bokor, E. Yablonovitch, and I. Siddiqi, A prototype silicon double quantum dot with dispersive microwave readout, *J. Appl. Phys.* **116**, 044503 (2014).
- [49] A. Rossi, R. Zhao, A. S. Dzurak, and M. F. Gonzalez-Zalba, Dispersive readout of a silicon quantum dot with an accumulation-mode gate sensor, *Appl. Phys. Lett.* **110**, 212101 (2017).
- [50] E. R. Eisenach, J. F. Barry, M. F. O’Keeffe, J. M. Schloss, M. H. Steinecker, D. R. Englund, and D. A. Braje, Cavity-enhanced microwave readout of a solid-state spin sensor, *Nat. Commun.* **12**, 1357 (2021).
- [51] J. A. Haigh, N. J. Lambert, A. C. Doherty, and A. J. Ferguson, Dispersive readout of ferromagnetic resonance for strongly coupled magnons and microwave photons, *Phys. Rev. B* **91**, 104410 (2015).
- [52] J. Ebel, T. Joas, M. Schalk, P. Weinbrenner, A. Angerer, J. Majer, and F. Reinhard, Dispersive readout of room-temperature ensemble spin sensors, *Quantum Sci. Technol.* **6**, 03LT01 (2021).
- [53] Á. Gómez-León, F. Luis, and D. Zueco, Dispersive readout of molecular spin qubits, *Phys. Rev. Appl.* **17**, 064030 (2022); Á. Gómez-León, Multiqudit interactions in molecular spins, *Phys. Rev. A* **106**, 022609 (2022).
- [54] N. E. Bousse, S. E. Kuenstner, J. M. L. Miller, H. K. Kwon, G. D. Vukasin, J. D. Teufel, and T. W. Kenny, Dispersive readout of a high-Q encapsulated micromechanical resonator, *Appl. Phys. Lett.* **121**, 073503 (2022).
- [55] G. Engelhardt and J. S. Cao, Dynamical symmetries and symmetry-protected selection rules in periodically driven quantum systems, *Phys. Rev. Lett.* **126**, 090601 (2021).
- [56] S. Kohler, Dispersive readout of adiabatic phases, *Phys. Rev. Lett.* **119**, 196802 (2017).
- [57] M. B. Chen, B. C. Wang, S. Kohler, Y. Kang, T. Lin, S. S. Gu, H. O. Li, G. C. Guo, X. D. Hu, H. W. Jiang, G. Cao, and G. P. Guo, Floquet state depletion in ac-driven circuit QED, *Phys. Rev. B* **103**, 205428 (2021).
- [58] B. D’Anjou and G. Burkard, Optimal dispersive readout of a spin qubit with a microwave resonator, *Phys. Rev. B* **100**, 245427 (2019).
- [59] J. Mielke, J. R. Petta, and G. Burkard, Nuclear spin readout in a cavity-coupled hybrid quantum dot-donor system, *PRX Quantum* **2**, 020347 (2021).
- [60] M. Malekakhlagh, E. Magesan, and L. C. G. Gavia, Time-dependent Schrieffer-Wolff-Lindblad perturbation theory: Measurement-induced dephasing and second-order Stark shift in dispersive readout, *Phys. Rev. A* **106**, 052601 (2022).
- [61] Z. Xiao, E. Doucet, T. Noh, L. Ranzani, R. W. Simmonds, L. C. G. Gavia, and A. Kamal, Perturbative diagonalization for time-dependent strong interactions, *Phys. Rev. Appl.* **18**, 024009 (2022).
- [62] M. Trif and P. Simon, Braiding of Majorana fermions in a cavity, *Phys. Rev. Lett.* **122**, 236803 (2019).
- [63] M. Boissonneault, J. M. Gambetta, and A. Blais, Improved superconducting qubit readout by qubit-induced nonlinearities, *Phys. Rev. Lett.* **105**, 100504 (2010).
- [64] T. Picot, A. Lupacscu, S. Saito, C. J. P. M. Harmans, and J. E. Mooij, Role of relaxation in the quantum measurement of a superconducting qubit using a nonlinear oscillator, *Phys. Rev. B* **78**, 132508 (2008).
- [65] J. C. Lee, W. D. Oliver, K. K. Berggren, and T. P. Orlando, Nonlinear resonant behavior of a dispersive readout circuit for a superconducting flux qubit, *Phys. Rev. B* **75**, 144505 (2007).
- [66] A. Lupacscu, E. F. C. Driessen, L. Roschier, C. J. P. M. Harmans, and J. E. Mooij, High-contrast dispersive readout of a superconducting flux qubit using a nonlinear resonator, *Phys. Rev. Lett.* **96**, 127003 (2006).
- [67] D. J. Ibberson, L. A. Ibberson, G. Smithson, J. A. Haigh, S. Barraud, and M. F. Gonzalez-Zalba, Low-temperature tunable radio-frequency resonator for sensitive dispersive readout of nanoelectronic devices, *Appl. Phys. Lett.* **114**, 123501 (2019).
- [68] F. Paolucci, P. Solinas, and F. Giazotto, Inductive superconducting quantum interference proximity transistor: The L-SQUIPT, *Phys. Rev. Appl.* **18**, 054042 (2022).
- [69] X. Wang, A. Miranowicz, and F. Nori, Ideal quantum non-demolition readout of a flux qubit without Purcell limitations, *Phys. Rev. Appl.* **12**, 064037 (2019).
- [70] J. D. Whittaker, F. C. S. da Silva, M. S. Allman, F. Lecocq, K. Cicak, A. J. Sirois, J. D. Teufel, J. Aumentado, and R. W. Simmonds, Tunable-cavity QED with phase qubits, *Phys. Rev. B* **90**, 024513 (2014).
- [71] W. Wustmann and V. Shumeiko, Parametric resonance in tunable superconducting cavities, *Phys. Rev. B* **87**, 184501 (2013).
- [72] J. E. Johnson, E. M. Hoskinson, C. Macklin, D. H. Slichter, I. Siddiqi, and J. Clarke, Dispersive readout of a flux qubit at the single-photon level, *Phys. Rev. B* **84**, 220503(R) (2011).
- [73] F. Foroughi, J. M. Mol, T. Müller, J. R. Kirtley, K. A. Moler, and H. Bluhm, A micro-SQUID with dispersive readout for magnetic scanning microscopy, *Appl. Phys. Lett.* **112**, 252601 (2018).
- [74] S. Michotte, Qubit dispersive readout scheme with a microstrip superconducting quantum interference device amplifier, *Appl. Phys. Lett.* **94**, 122512 (2009).
- [75] G. Liu, X. Cao, T. C. Chien, C. Zhou, P. Lu, and M. Hatridge, Noise reduction in qubit readout with a two-mode squeezed interferometer, *Phys. Rev. Appl.* **18**, 064092 (2022).

- [76] A. Vaaranta, M. Cattaneo, and R. E. Lake, Dynamics of a dispersively coupled transmon qubit in the presence of a noise source embedded in the control line, *Phys. Rev. A* **106**, 042605 (2022).
- [77] S. Majumder, T. Bera, and V. Singh, Prospects of cooling a mechanical resonator with a transmon qubit in c-QED setup, *Phys. Rev. Res.* **4**, 033232 (2022).
- [78] Y. Sunada, S. Kono, J. Ilves, S. Tamate, T. Sugiyama, Y. Tabuchi, and Y. Nakamura, Fast readout and reset of a superconducting qubit coupled to a resonator with an intrinsic Purcell filter, *Phys. Rev. Appl.* **17**, 044016 (2022).
- [79] K. Rudinger, G. J. Ribeill, L. C. G. Govia, M. Ware, E. Nielsen, K. Young, T. A. Ohki, R. Blume-Kohout, and T. Proctor, Characterizing midcircuit measurements on a superconducting qubit using gate set tomography, *Phys. Rev. Appl.* **17**, 014014 (2022).
- [80] Y. F. Ye, K. D. Peng, M. Naghiloo, G. Cunningham, and K. P. O'Brien, Engineering purely nonlinear coupling between superconducting qubits using a quarton, *Phys. Rev. Lett.* **127**, 050502 (2021).
- [81] G. Angelatos, S. A. Khan, and H. E. Türeci, Reservoir computing approach to quantum state measurement, *Phys. Rev. X* **11**, 041062 (2021).
- [82] D. Pitsun, A. Sultanov, I. Novikov, E. Mutsenik, B. Ivanov, A. Matanin, V. Polozov, E. Malevannaya, A. Ivanov, G. Fedorov, K. Delfanazari, I. Rodionov, and E. Il'ichev, Cross coupling of a solid-state qubit to an input signal due to multiplexed dispersive readout, *Phys. Rev. Appl.* **14**, 054059 (2020).
- [83] J. C. Pommerening and D. P. DiVincenzo, What is measured when a qubit measurement is performed on a multiqubit chip, *Phys. Rev. A* **102**, 032623 (2020).
- [84] T. Peronnin, D. Marković, Q. Ficheux, and B. Huard, Sequential dispersive measurement of a superconducting qubit, *Phys. Rev. Lett.* **124**, 180502 (2020).
- [85] R. Dassonneville, T. Ramos, V. Milchakov, L. Planat, É. Dumur, F. Foroughi, J. Puertas, S. Leger, K. Bharadwaj, J. Delaforce, C. Naud, W. Hasch-Guichard, J. J. García-Ripoll, N. Roch, and O. Buisson, Fast high-fidelity quantum non-demolition qubit readout via a nonperturbative cross-Kerr coupling, *Phys. Rev. X* **10**, 011045 (2020).
- [86] A. D. Patterson, J. Rahamim, T. Tsunoda, P. A. Spring, S. Jebari, K. Ratter, M. Mergenthaler, G. Tancredi, B. Vlastakis, M. Esposito, and P. J. Leek, Calibration of a cross-resonance two-qubit gate between directly coupled transmons, *Phys. Rev. Appl.* **12**, 064013 (2019).
- [87] K. Serniak, S. Diamond, M. Hays, V. Fatemi, S. Shankar, L. Frunzio, R. J. Schoelkopf, and M. H. Devoret, Direct dispersive monitoring of charge parity in offset-charge-sensitive transmons, *Phys. Rev. Appl.* **12**, 014052 (2019).
- [88] J. Ikonen, J. Goetz, J. Ilves, A. Keränen, A. M. Gunyho, M. Partanen, K. Y. Tan, D. Hazra, L. Grönberg, V. Vesterinen, S. Simbierowicz, J. Hassel, and M. Möttönen, Qubit measurement by multichannel driving, *Phys. Rev. Lett.* **122**, 080503 (2019).
- [89] C. T. Hann, S. S. Elder, C. S. Wang, K. Chou, R. J. Schoelkopf, and L. Jiang, Robust readout of bosonic qubits in the dispersive coupling regime, *Phys. Rev. A* **98**, 022305 (2018).
- [90] T. Walter, P. Kurpiers, S. Gasparinetti, P. Magnard, A. Potočnik, Y. Salathé, M. Pechal, M. Mondal, M. Oppliger, C. Eichler, and A. Wallraff, Rapid high-fidelity single-shot dispersive readout of superconducting qubits, *Phys. Rev. Appl.* **7**, 054020 (2017).
- [91] A. Sokolov, Optimal conditions for high-fidelity dispersive readout of a qubit with a photon-number-resolving detector, *Phys. Rev. A* **93**, 032323 (2016); H. Z. Shen, Y. H. Zhou, H. D. Liu, G. C. Wang, and X. X. Yi, Exact optimal control of photon blockade with weakly nonlinear coupled cavities, *Opt. Express* **23**, 32835 (2015); W. S. Xue, H. Z. Shen, and X. X. Yi, Nonreciprocal conventional photon blockade in driven dissipative atom-cavity, *Opt. Lett.* **45**, 4424 (2020).
- [92] N. Didier, J. Bourassa, and A. Blais, Fast quantum non-demolition readout by parametric modulation of longitudinal qubit-oscillator interaction, *Phys. Rev. Lett.* **115**, 203601 (2015).
- [93] S. E. Nigg and S. M. Girvin, Stabilizer quantum error correction toolbox for superconducting qubits, *Phys. Rev. Lett.* **110**, 243604 (2013).
- [94] E. A. Sete, A. Galiutdinov, E. Mlinar, J. M. Martinis, and A. N. Korotkov, Catch-disperse-release readout for superconducting qubits, *Phys. Rev. Lett.* **110**, 210501 (2013).
- [95] K. Inomata, T. Yamamoto, P. M. Billangeon, Y. Nakamura, and J. S. Tsai, Large dispersive shift of cavity resonance induced by a superconducting flux qubit in the straddling regime, *Phys. Rev. B* **86**, 140508(R) (2012).
- [96] E. Rinaldi, R. D. Candia, S. Felicetti, and F. Minganti, Dispersive qubit readout with machine learning, [arXiv:2112.05332](https://arxiv.org/abs/2112.05332).
- [97] B. D'Anjou, Generalized figure of merit for qubit readout, *Phys. Rev. A* **103**, 042404 (2021).
- [98] Z. R. Lin, K. Inomata, K. Koshino, W. D. Oliver, Y. Nakamura, J. S. Tsai, and T. Yamamoto, Josephson parametric phase-locked oscillator and its application to dispersive readout of superconducting qubits, *Nat. Commun.* **5**, 4480 (2014).
- [99] Y. Chen, D. Sank, P. O'Malley, T. White, R. Barends, B. Chiaro, J. Kelly, E. Lucero, M. Mariantoni, A. Megrant, C. Neill, A. Vainsencher, J. Wenner, Y. Yin, A. N. Cleland, and J. M. Martinis, Multiplexed dispersive readout of superconducting phase qubits, *Appl. Phys. Lett.* **101**, 182601 (2012).
- [100] S. Indrajeet, H. Wang, M. D. Hutchings, B. G. Taketani, F. K. Wilhelm, M. D. Lahaye, and B. L. T. Plourde, Coupling a superconducting qubit to a left-handed metamaterial resonator, *Phys. Rev. Appl.* **14**, 064033 (2020).
- [101] I. Siddiqi, R. Vijay, M. Metcalfe, E. Boaknin, L. Frunzio, R. J. Schoelkopf, and M. H. Devoret, Dispersive measurements of superconducting qubit coherence with a fast latching readout, *Phys. Rev. B* **73**, 054510 (2006).
- [102] I. Serban, E. Solano, and F. K. Wilhelm, Phase-space theory for dispersive detectors of superconducting qubits, *Phys. Rev. B* **76**, 104510 (2007).
- [103] M. Baur, S. Filipp, R. Bianchetti, J. M. Fink, M. Göppl, L. Steffen, P. J. Leek, A. Blais, and A. Wallraff, Measurement of Autler-Townes and Mollow transitions in a strongly driven superconducting qubit, *Phys. Rev. Lett.* **102**, 243602 (2009).
- [104] A. Eddins, S. Schreppler, D. M. Toyli, L. S. Martin, S. Hacohe-Gourgy, L. C. G. Govia, H. Ribeiro, A. A. Clerk, and I. Siddiqi, Stroboscopic qubit measurement with squeezed illumination, *Phys. Rev. Lett.* **120**, 040505 (2018).
- [105] M. Metcalfe, E. Boaknin, V. Manucharyan, R. Vijay, I. Siddiqi, C. Rigetti, L. Frunzio, R. J. Schoelkopf, and M. H. Devoret, Measuring the decoherence of a quantum qubit

- with the cavity bifurcation amplifier, *Phys. Rev. B* **76**, 174516 (2007).
- [106] G. Oelsner, S. H. W. van der Ploeg, P. Macha, U. Hübner, D. Born, S. Anders, E. Il'ichev, H. G. Meyer, M. Grajcar, S. Wünsch, M. Siegel, A. N. Omelyanchouk, and O. Astafiev, Weak continuous monitoring of a flux qubit using coplanar waveguide resonator, *Phys. Rev. B* **81**, 172505 (2010).
- [107] R. Mizuta, R. M. Otxoa, A. C. Betz, and M. F. Gonzalez-Zalba, Quantum and tunneling capacitance in charge and spin qubits, *Phys. Rev. B* **95**, 045414 (2017).
- [108] T. B. Smith, M. C. Cassidy, D. J. Reilly, S. D. Bartlett, and A. L. Grimsmo, Dispersive readout of Majorana qubits, *PRX Quantum* **1**, 020313 (2020).
- [109] V. D. Maman, M. F. Gonzalez-Zalba, and A. Pályi, Charge noise and overdrive errors in reflectometry-based charge, spin and Majorana qubit readout, *Phys. Rev. Appl.* **14**, 064024 (2020).
- [110] D. Gusenkova, M. Spiecker, R. Gebauer, M. Willsch, D. Willsch, F. Valenti, N. Karcher, L. Grünhaupt, I. Takmakov, P. Winkel, D. Rieger, A. V. Ustinov, N. Roch, W. Wernsdorfer, K. Michielsen, O. Sander, and I. M. Pop, Quantum nondemolition dispersive readout of a superconducting artificial atom using large photon numbers, *Phys. Rev. Appl.* **15**, 064030 (2021).
- [111] G. P. Fedorov, V. B. Yursa, A. E. Efimov, K. I. Shiiyanov, A. Y. Dmitriev, I. A. Rodionov, A. A. Dobronosova, D. O. Moskalev, A. A. Pishchimova, E. I. Malevannaya, and O. V. Astafiev, Light dressing of a diatomic superconducting artificial molecule, *Phys. Rev. A* **102**, 013707 (2020).
- [112] R. Bianchetti, S. Filipp, M. Baur, J. M. Fink, C. Lang, L. Steffen, M. Boissonneault, A. Blais, and A. Wallraff, Control and tomography of a three level superconducting artificial atom, *Phys. Rev. Lett.* **105**, 223601 (2010).
- [113] I. Diniz, E. Dumur, O. Buisson, and A. Auffèves, Ultrafast quantum nondemolition measurements based on a diamond-shaped artificial atom, *Phys. Rev. A* **87**, 033837 (2013).
- [114] I. Takmakov, P. Winkel, F. Foroughi, L. Planat, D. Gusenkova, M. Spiecker, D. Rieger, L. Grünhaupt, A. V. Ustinov, W. Wernsdorfer, I. M. Pop, and N. Roch, Minimizing the discrimination time for quantum states of an artificial atom, *Phys. Rev. Appl.* **15**, 064029 (2021).
- [115] M. Benito, X. Mi, J. M. Taylor, J. R. Petta, and G. Burkard, Input-output theory for spin-photon coupling in Si double quantum dots, *Phys. Rev. B* **96**, 235434 (2017).
- [116] G. Burkard and J. R. Petta, Dispersive readout of valley splittings in cavity-coupled silicon quantum dots, *Phys. Rev. B* **94**, 195305 (2016).
- [117] T. Niemczyk, F. Deppe, H. Huebl, E. P. Menzel, F. Hocke, M. J. Schwarz, J. J. García-Ripoll, D. Zueco, T. Hümmer, E. Solano, A. Marx, and R. Gross, Circuit quantum electrodynamics in the ultrastrong-coupling regime, *Nat. Phys.* **6**, 772 (2010).
- [118] P. Forn-Díaz, J. Lisenfeld, D. Marcos, J. J. García-Ripoll, E. Solano, C. J. P. M. Harmans, and J. E. Mooij, Observation of the Bloch-Siegert shift in a qubit-oscillator system in the ultrastrong coupling regime, *Phys. Rev. Lett.* **105**, 237001 (2010).
- [119] P. Forn-Díaz, J. J. García-Ripoll, B. Peropadre, J. L. Orgiazzi, M. A. Yurtalan, R. Belyansky, C. M. Wilson, and A. Lupascu, Ultrastrong coupling of a single artificial atom to an electro-magnetic continuum in the nonperturbative regime, *Nat. Phys.* **13**, 39 (2017).
- [120] Z. Chen, Y. M. Wang, T. F. Li, L. Tian, Y. Y. Qiu, K. Inomata, F. Yoshihara, S. Y. Han, F. Nori, J. S. Tsai, and J. Q. You, Single-photon-driven high-order sideband transitions in an ultrastrongly coupled circuit-quantum-electrodynamics system, *Phys. Rev. A* **96**, 012325 (2017).
- [121] F. Yoshihara, T. Fuse, S. Ashhab, K. Kakuyanagi, S. Saito, and K. Semba, Superconducting qubit-oscillator circuit beyond the ultrastrong-coupling regime, *Nat. Phys.* **13**, 44 (2017).
- [122] H. Z. Shen, Q. Wang, and X. X. Yi, Dispersive readout with non-Markovian environments, *Phys. Rev. A* **105**, 023707 (2022).
- [123] S. Kohler, Dispersive readout: Universal theory beyond the rotating-wave approximation, *Phys. Rev. A* **98**, 023849 (2018).
- [124] D. Zueco, G. M. Reuther, S. Kohler, and P. Hänggi, Qubit-oscillator dynamics in the dispersive regime: Analytical theory beyond the rotating-wave approximation, *Phys. Rev. A* **80**, 033846 (2009).
- [125] A. M. Sokolov and E. V. Stolyarov, Single-photon limit of dispersive readout of a qubit with a photodetector, *Phys. Rev. A* **101**, 042306 (2020).
- [126] V. L. Grigoryan and K. Xia, Cavity-mediated dissipative spin-spin coupling, *Phys. Rev. B* **100**, 014415 (2019).
- [127] P. C. Xu, J. W. Rao, Y. S. Gui, X. F. Jin, and C. M. Hu, Cavity-mediated dissipative coupling of distant magnetic moments: Theory and experiment, *Phys. Rev. B* **100**, 094415 (2019).
- [128] X. F. Zhang, C. L. Zou, L. Jiang, and H. X. Tang, Strongly coupled magnons and cavity microwave photons, *Phys. Rev. Lett.* **113**, 156401 (2014).
- [129] J. Zhao, L. H. Wu, T. F. Li, Y. X. Liu, F. Nori, Y. L. Liu, and J. F. Du, Phase-controlled pathway interferences and switchable fast-slow light in a cavity-magnon polariton system, *Phys. Rev. Appl.* **15**, 024056 (2021).
- [130] G. G. Zhao, Y. Wang, and X. F. Qian, Driven dissipative quantum dynamics in a cavity magnon-polariton system, *Phys. Rev. B* **104**, 134423 (2021).
- [131] M. Harder, Y. Yang, B. M. Yao, C. H. Yu, J. W. Rao, Y. S. Gui, R. L. Stamps, and C. M. Hu, Level attraction due to dissipative magnon-photon coupling, *Phys. Rev. Lett.* **121**, 137203 (2018).
- [132] V. L. Grigoryan, K. Shen, and K. Xia, Synchronized spin-photon coupling in a microwave cavity, *Phys. Rev. B* **98**, 024406 (2018).
- [133] B. Bhoi, B. Kim, S. H. Jang, J. Kim, J. Yang, Y. J. Cho, and S. K. Kim, Abnormal anticrossing effect in photon-magnon coupling, *Phys. Rev. B* **99**, 134426 (2019).
- [134] V. L. Grigoryan and K. Xia, Thermally induced monochromatic microwave generation in magnon polaritons, *Phys. Rev. B* **99**, 224408 (2019).
- [135] W. C. Yu, J. J. Wang, H. Y. Yuan, and J. Xiao, Prediction of attractive level crossing via a dissipative mode, *Phys. Rev. Lett.* **123**, 227201 (2019).
- [136] I. Boventer, C. Dörflinger, T. Wolz, R. Macêdo, R. Lebrun, M. Kläui, and M. Weides, Control of the coupling strength and linewidth of a cavity magnon-polariton, *Phys. Rev. Res.* **2**, 013154 (2020).
- [137] Y. Tabuchi, S. Ishino, T. Ishikawa, R. Yamazaki, K. Usami, and Y. Nakamura, Hybridizing ferromagnetic magnons and microwave photons in the quantum limit, *Phys. Rev. Lett.* **113**,

- 083603 (2014); L. H. Bai, M. Harder, Y. P. Chen, X. Fan, J. Q. Xiao, and C. M. Hu, Spin pumping in electro-dynamically coupled magnon-photon systems, *ibid.* **114**, 227201 (2015).
- [138] M. Goryachev, W. G. Farr, D. L. Creedon, Y. Fan, M. Kostylev, and M. E. Tobar, High-cooperativity cavity QED with magnons at microwave frequencies, *Phys. Rev. Appl.* **2**, 054002 (2014); H. Huebl, C. W. Zollitsch, J. Lotze, F. Hocke, M. Greifenstein, A. Marx, R. Gross, and S. T. B. Goennenwein, High cooperativity in coupled microwave resonator ferrimagnetic insulator hybrids, *Phys. Rev. Lett.* **111**, 127003 (2013).
- [139] H. Y. Yuan, P. Yan, S. S. Zheng, Q. Y. He, K. Xia, and M. H. Yung, Steady Bell state generation via magnon-photon coupling, *Phys. Rev. Lett.* **124**, 053602 (2020).
- [140] F. Troiani, Readout of a weakly coupled qubit through the use of an auxiliary mode, *Phys. Lett. A* **383**, 1536 (2019).
- [141] F. Quijandría, U. Naether, S. K. Özdemir, F. Nori, and D. Zueco, \mathcal{PT} -symmetric circuit QED, *Phys. Rev. A* **97**, 053846 (2018).
- [142] C. M. Bender and S. Boettcher, Real spectra in non-Hermitian Hamiltonians having \mathcal{PT} symmetry, *Phys. Rev. Lett.* **80**, 5243 (1998).
- [143] A. Mostafazadeh, Pseudo-Hermiticity versus PT symmetry: The necessary condition for the reality of the spectrum of a non-Hermitian Hamiltonian, *J. Math. Phys.* **43**, 205 (2002).
- [144] A. Mostafazadeh, Pseudo-Hermiticity versus PT-symmetry. II. A complete characterization of non-Hermitian Hamiltonians with a real spectrum, *J. Math. Phys.* **43**, 2814 (2002).
- [145] A. Mostafazadeh, Pseudo-Hermiticity versus PT-symmetry III: Equivalence of pseudo-Hermiticity and the presence of antilinear symmetries, *J. Math. Phys.* **43**, 3944 (2002).
- [146] C. M. Bender, Introduction to \mathcal{PT} -symmetric quantum theory, *Contemp. Phys.* **46**, 277 (2005).
- [147] C. M. Bender, Making sense of non-Hermitian Hamiltonians, *Rep. Prog. Phys.* **70**, 947 (2007).
- [148] V. L. Grigoryan and K. Xia, Torque-induced dispersive readout in a weakly coupled hybrid system, *Phys. Rev. B* **102**, 064426 (2020).
- [149] V. V. Konotop, J. K. Yang, and D. A. Zezyulin, Nonlinear waves in \mathcal{PT} -symmetric systems, *Rev. Mod. Phys.* **88**, 035002 (2016).
- [150] W. D. Heiss, The physics of exceptional points, *J. Phys. A: Math. Theor.* **45**, 444016 (2012).
- [151] T. X. Lu, H. L. Zhang, Q. Zhang, and H. Jing, Exceptional-point-engineered cavity magnomechanics, *Phys. Rev. A* **103**, 063708 (2021).
- [152] Z. Lin, A. Pick, M. Lončar, and A. W. Rodríguez, Enhanced spontaneous emission at third-order dirac exceptional points in inverse-designed photonic crystals, *Phys. Rev. Lett.* **117**, 107402 (2016).
- [153] X. Y. Lü, H. Jing, J. Y. Ma, and Y. Wu, \mathcal{PT} -symmetry-breaking chaos in optomechanics, *Phys. Rev. Lett.* **114**, 253601 (2015).
- [154] L. Feng, Y. L. Xu, W. S. Fegadolli, M. H. Lu, J. E. B. Oliveira, V. R. Almeida, Y. F. Chen, and A. Scherer, Experimental demonstration of a unidirectional reflectionless parity-time metamaterial at optical frequencies, *Nat. Mater.* **12**, 108 (2013).
- [155] Z. Lin, H. Ramezani, T. Eichelkraut, T. Kottos, H. Cao, and D. N. Christodoulides, Unidirectional invisibility induced by \mathcal{PT} -symmetric periodic structures, *Phys. Rev. Lett.* **106**, 213901 (2011).
- [156] L. Feng, Z. J. Wong, R. M. Ma, Y. Wang, and X. Zhang, Single-mode laser by parity-time symmetry breaking, *Science* **346**, 972 (2014).
- [157] H. Hodaei, M. A. Miri, M. Heinrich, D. N. Christodoulides, and M. Khajavikhan, Parity-time-symmetric microring lasers, *Science* **346**, 975 (2014).
- [158] M. Liertzer, L. Ge, A. Cerjan, A. D. Stone, H. E. Türeci, and S. Rotter, Pump-induced exceptional points in lasers, *Phys. Rev. Lett.* **108**, 173901 (2012).
- [159] Z. P. Liu, J. Zhang, Ş. K. Özdemir, B. Peng, H. Jing, X. Y. Lü, C. W. Li, L. Yang, F. Nori, and Y. X. Liu, Metrology with \mathcal{PT} -symmetric cavities: Enhanced sensitivity near the \mathcal{PT} -phase transition, *Phys. Rev. Lett.* **117**, 110802 (2016).
- [160] J. H. Li, R. Yu, and Y. Wu, Proposal for enhanced photon blockade in parity-time-symmetric coupled microcavities, *Phys. Rev. A* **92**, 053837 (2015); Y. H. Zhou, H. Z. Shen, and X. X. Yi, Unconventional photon blockade with second-order nonlinearity, *ibid.* **92**, 023838 (2015); H. Z. Shen, Y. H. Zhou, and X. X. Yi, Tunable photon blockade in coupled semiconductor cavities, *ibid.* **91**, 063808 (2015); Quantum optical diode with semiconductor microcavities, **90**, 023849 (2014).
- [161] J. Wiersig, Enhancing the sensitivity of frequency and energy splitting detection by using exceptional points: Application to microcavity sensors for single-particle detection, *Phys. Rev. Lett.* **112**, 203901 (2014).
- [162] T. D. Ladd, F. Jelezko, R. Laflamme, Y. Nakamura, C. Monroe, and J. L. O'Brien, Quantum computers, *Nature (London)* **464**, 45 (2010).
- [163] H. P. Breuer and F. Petruccione, *The Theory of Open Quantum Systems* (Oxford University Press, Oxford, 2002).
- [164] U. Weiss, *Quantum Dissipative Systems*, 3rd ed. (World Scientific, Singapore, 2008).
- [165] F. Caruso, V. Giovannetti, C. Lupo, and S. Mancini, Quantum channels and memory effects, *Rev. Mod. Phys.* **86**, 1203 (2014).
- [166] C. W. Gardiner and P. Zoller, *Quantum Noise* (Springer, Berlin, 2000).
- [167] J. G. Li, J. Zou, and B. Shao, Non-Markovianity of the damped Jaynes-Cummings model with detuning, *Phys. Rev. A* **81**, 062124 (2010); H. Z. Shen, M. Qin, and X. X. Yi, Single-photon storing in coupled non-Markovian atom-cavity system, *ibid.* **88**, 033835 (2013); H. Z. Shen, Y. Chen, T. Z. Luan, and X. X. Yi, Multiple single-photon generations in three-level atoms coupled to cavity with non-Markovian effects, *ibid.* **107**, 053705 (2023).
- [168] R. Lo Franco, B. Bellomo, S. Maniscalco, and G. Compagno, Dynamics of quantum correlations in two-qubit systems within non-Markovian environments, *Int. J. Mod. Phys. B* **27**, 1345053 (2013).
- [169] G. M. Reuther, P. Hänggi, and S. Kohler, Non-Markovian qubit decoherence during dispersive readout, *Phys. Rev. A* **85**, 062123 (2012).
- [170] V. Link, K. Müller, R. G. Lena, K. Luoma, F. Damanet, W. T. Strunz, and A. J. Daley, Non-Markovian quantum dynamics in strongly coupled multimode cavities conditioned on continuous measurement, *PRX Quantum* **3**, 020348 (2022).

- [171] A. Burgess and M. Florescu, Non-Markovian dynamics of a single excitation within many-body dissipative systems, *Phys. Rev. A* **105**, 062207 (2022); U. Hoeppe, C. Wolff, J. Küchenmeister, J. Niegemann, M. Drescher, H. Benner, and K. Busch, Direct observation of non-Markovian radiation dynamics in 3D bulk photonic crystals, *Phys. Rev. Lett.* **108**, 043603 (2012).
- [172] J. I. Costa-Filho, R. B. B. Lima, R. R. Paiva, P. M. Soares, W. A. M. Morgado, R. Lo Franco, and D. O. Soares-Pinto, Enabling quantum non-Markovian dynamics by injection of classical colored noise, *Phys. Rev. A* **95**, 052126 (2017).
- [173] K. W. Chang and C. K. Law, Non-Markovian master equation for a damped oscillator with time-varying parameters, *Phys. Rev. A* **81**, 052105 (2010); S. Longhi, Non-Markovian decay and lasing condition in an optical microcavity coupled to a structured reservoir, *ibid.* **74**, 063826 (2006); H. T. Tan and W. M. Zhang, Non-Markovian dynamics of an open quantum system with initial system-reservoir correlations: A nanocavity coupled to a coupled-resonator optical waveguide, *ibid.* **83**, 032102 (2011).
- [174] I. de Vega and D. Alonso, Dynamics of non-Markovian open quantum systems, *Rev. Mod. Phys.* **89**, 015001 (2017); H. Z. Shen, J. F. Yang, and X. X. Yi, Unconventional photon blockade with non-Markovian effects in driven dissipative coupled cavities, *Phys. Rev. A* **109**, 043714 (2024); W. Zhang and H. Z. Shen, Optomechanical second-order sidebands and group delays in a spinning resonator with a parametric amplifier and non-Markovian effects, *ibid.* **109**, 033701 (2024).
- [175] B. H. Liu, L. Li, Y. F. Huang, C. F. Li, G. C. Guo, E. M. Laine, H. P. Breuer, and J. Piilo, Experimental control of the transition from Markovian to non-Markovian dynamics of open quantum systems, *Nat. Phys.* **7**, 931 (2011); S. J. Xiong, Q. W. Hu, Z. Sun, L. Yu, Q. P. Su, J. M. Liu, and C. P. Yang, Non-Markovianity in experimentally simulated quantum channels: Role of counterrotating-wave terms, *Phys. Rev. A* **100**, 032101 (2019); S. Cialdi, C. Benedetti, D. Tamascelli, S. Olivares, M. G. A. Paris, and B. Vacchini, Experimental investigation of the effect of classical noise on quantum non-Markovian dynamics, *ibid.* **100**, 052104 (2019).
- [176] D. Khurana, B. K. Agarwalla, and T. S. Mahesh, Experimental emulation of quantum non-Markovian dynamics and coherence protection in the presence of information backflow, *Phys. Rev. A* **99**, 022107 (2019).
- [177] K. H. Madsen, S. Ates, T. Lund-Hansen, A. Löffler, S. Reitzenstein, A. Forchel, and P. Lodahl, Observation of non-Markovian dynamics of a single quantum dot in a micropillar cavity, *Phys. Rev. Lett.* **106**, 233601 (2011).
- [178] Y. Guo, P. Taranto, B. H. Liu, X. M. Hu, Y. F. Huang, C. F. Li, and G. C. Guo, Experimental demonstration of instrument-specific quantum memory effects and non-Markovian process recovery for common-cause processes, *Phys. Rev. Lett.* **126**, 230401 (2021).
- [179] B. W. Li, Q. X. Mei, Y. K. Wu, M. L. Cai, Y. Wang, L. Yao, Z. C. Zhou, and L. M. Duan, Observation of non-Markovian spin dynamics in a Jaynes-Cummings-Hubbard model using a trapped-ion quantum simulator, *Phys. Rev. Lett.* **129**, 140501 (2022); J. S. Xu, C. F. Li, C. J. Zhang, X. Y. Xu, Y. S. Zhang, and G. C. Guo, Experimental investigation of the non-Markovian dynamics of classical and quantum correlations, *Phys. Rev. A* **82**, 042328 (2010); J. S. Tang, C. F. Li, Y. L. Li, X. B. Zou, G. C. Guo, H. P. Breuer, E. M. Laine, and J. Piilo, Measuring non-Markovianity of processes with controllable system-environment interaction, *Europhys. Lett.* **97**, 10002 (2012).
- [180] S. A. Uriri, F. Wudarski, I. Sinayskiy, F. Petruccione, and M. S. Tame, Experimental investigation of Markovian and non-Markovian channel addition, *Phys. Rev. A* **101**, 052107 (2020).
- [181] M. H. Anderson, G. Vemuri, J. Cooper, P. Zoller, and S. J. Smith, Experimental study of absorption and gain by two-level atoms in a time-delayed non-Markovian optical field, *Phys. Rev. A* **47**, 3202 (1993).
- [182] Z. D. Liu, Y. N. Sun, B. H. Liu, C. F. Li, G. C. Guo, S. Hamedani Raja, H. Lyyra, and J. Piilo, Experimental realization of high-fidelity teleportation via a non-Markovian open quantum system, *Phys. Rev. A* **102**, 062208 (2020).
- [183] B. Bylicka, D. Chruściński, and S. Maniscalco, Non-Markovianity and reservoir memory of quantum channels: A quantum information theory perspective, *Sci. Rep.* **4**, 5720 (2014); H. Z. Shen, S. Xu, H. T. Cui, and X. X. Yi, Non-Markovian dynamics of a system of two-level atoms coupled to a structured environment, *Phys. Rev. A* **99**, 032101 (2019); L. Xin, S. Xu, X. X. Yi, and H. Z. Shen, Tunable non-Markovian dynamics with a three-level atom mediated by the classical laser in a semi-infinite photonic waveguide, *ibid.* **105**, 053706 (2022).
- [184] S. B. Xue, R. B. Wu, W. M. Zhang, J. Zhang, C. W. Li, and T. J. Tarn, Decoherence suppression via non-Markovian coherent feedback control, *Phys. Rev. A* **86**, 052304 (2012).
- [185] H. P. Breuer, E. M. Laine, J. Piilo, and B. Vacchini, Colloquium: Non-Markovian dynamics in open quantum systems, *Rev. Mod. Phys.* **88**, 021002 (2016).
- [186] H. P. Breuer, E. M. Laine, and J. Piilo, Measure for the degree of non-Markovian behavior of quantum processes in open systems, *Phys. Rev. Lett.* **103**, 210401 (2009); E. M. Laine, J. Piilo, and H. P. Breuer, Measure for the non-Markovianity of quantum processes, *Phys. Rev. A* **81**, 062115 (2010); C. Addis, B. Bylicka, D. Chruściński, and S. Maniscalco, Comparative study of non-Markovianity measures in exactly solvable one- and two-qubit models, *ibid.* **90**, 052103 (2014).
- [187] S. Wißmann, A. Karlsson, E. M. Laine, J. Piilo, and H. P. Breuer, Optimal state pairs for non-Markovian quantum dynamics, *Phys. Rev. A* **86**, 062108 (2012).
- [188] S. Wißmann, H. P. Breuer, and B. Vacchini, Generalized trace-distance measure connecting quantum and classical non-Markovianity, *Phys. Rev. A* **92**, 042108 (2015).
- [189] S. Lorenzo, F. Plastina, and M. Paternostro, Geometrical characterization of non-Markovianity, *Phys. Rev. A* **88**, 020102(R) (2013).
- [190] A. Rivas, S. F. Huelga, and M. B. Plenio, Entanglement and non-Markovianity of quantum evolutions, *Phys. Rev. Lett.* **105**, 050403 (2010); S. L. Luo, S. S. Fu, and H. T. Song, Quantifying non-Markovianity via correlations, *Phys. Rev. A* **86**, 044101 (2012); M. M. Wolf, J. Eisert, T. S. Cubitt, and J. I. Cirac, Assessing non-Markovian quantum dynamics, *Phys. Rev. Lett.* **101**, 150402 (2008); X. M. Lu, X. G. Wang, and C. P. Sun, Quantum Fisher information flow and non-Markovian processes of open systems, *Phys. Rev. A* **82**, 042103 (2010); D. Chruściński and S. Maniscalco, Degree of

- non-Markovianity of quantum evolution, *Phys. Rev. Lett.* **112**, 120404 (2014).
- [191] M. O. Scully and M. S. Zubairy, *Quantum Optics* (Cambridge University Press, Cambridge, 1997).
- [192] D. F. Walls and G. J. Milburn, *Quantum Optics*, 2nd ed. (Springer, Berlin, 2008).
- [193] J. R. Schrieffer and P. A. Wolff, Relation between the Anderson and Kondo Hamiltonians, *Phys. Rev.* **149**, 491 (1966).
- [194] V. Srinivasa, J. M. Taylor, and C. Tahan, Entangling distant resonant exchange qubits via circuit quantum electrodynamics, *Phys. Rev. B* **94**, 205421 (2016); P. Zhao, P. Xu, D. Lan, X. S. Tan, H. F. Yu, and Y. Yu, Switchable next-nearest-neighbor coupling for controlled two-qubit operations, *Phys. Rev. Appl.* **14**, 064016 (2020).
- [195] D. I. Schuster, A. Wallraff, A. Blais, L. Frunzio, R. S. Huang, J. Majer, S. M. Girvin, and R. J. Schoelkopf, ac Stark shift and dephasing of a superconducting qubit strongly coupled to a cavity field, *Phys. Rev. Lett.* **94**, 123602 (2005).
- [196] H. Hodaie, A. U. Hassan, S. Wittek, H. Garcia-Gracia, R. El-Ganainy, D. N. Christodoulides, and M. Khajavikhan, Enhanced sensitivity at higher-order exceptional points, *Nature (London)* **548**, 187 (2017).
- [197] W. J. Chen, Ş. K. Özdemir, G. M. Zhao, J. Wiersig, and L. Yang, Exceptional points enhance sensing in an optical microcavity, *Nature (London)* **548**, 192 (2017).
- [198] C. Uchiyama, M. Aihara, M. Saeki, and S. Miyashita, Master equation approach to line shape in dissipative systems, *Phys. Rev. E* **80**, 021128 (2009).
- [199] M. Saeki, C. Uchiyama, T. Mori, and S. Miyashita, Comparison among various expressions of complex admittance for quantum systems in contact with a heat reservoir, *Phys. Rev. E* **81**, 031131 (2010).
- [200] H. Z. Shen, M. Qin, X. Q. Shao, and X. X. Yi, General response formula and application to topological insulator in quantum open system, *Phys. Rev. E* **92**, 052122 (2015).
- [201] A. A. Clerk, M. H. Devoret, S. M. Girvin, F. Marquardt, and R. J. Schoelkopf, Introduction to quantum noise, measurement, and amplification, *Rev. Mod. Phys.* **82**, 1155 (2010).
- [202] J. Zhang, Y. X. Liu, R. B. Wu, K. Jacobs, and F. Nori, Non-Markovian quantum input-output networks, *Phys. Rev. A* **87**, 032117 (2013).
- [203] L. Diósi, Non-Markovian open quantum systems: Input-output fields, memory, and monitoring, *Phys. Rev. A* **85**, 034101 (2012).
- [204] M. W. Jack and J. J. Hope, Resonance fluorescence in a band-gap material: Direct numerical simulation of non-Markovian evolution, *Phys. Rev. A* **63**, 043803 (2001).
- [205] S. Gröblacher, A. Trubarov, N. Prigge, G. D. Cole, M. Aspelmeyer, and J. Eisert, Observation of non-Markovian micromechanical Brownian motion, *Nat. Commun.* **6**, 7606 (2015).
- [206] H. N. Xiong, W. M. Zhang, M. W. Y. Tu, and D. Braun, Dynamically stabilized decoherence-free states in non-Markovian open fermionic systems, *Phys. Rev. A* **86**, 032107 (2012).
- [207] H. Z. Shen, D. X. Li, and X. X. Yi, Non-Markovian linear response theory for quantum open systems and its applications, *Phys. Rev. E* **95**, 012156 (2017).
- [208] J. Jing and T. Yu, Non-Markovian relaxation of a three-level system: Quantum trajectory approach, *Phys. Rev. Lett.* **105**, 240403 (2010); Z. Y. Li and H. Z. Shen, Non-Markovian dynamics with a giant atom coupled to a semi-infinite photonic waveguide, *Phys. Rev. A* **109**, 023712 (2024); H. Z. Shen, X. Q. Shao, G. C. Wang, X. L. Zhao, and X. X. Yi, Quantum phase transition in a coupled two-level system embedded in anisotropic three-dimensional photonic crystals, *Phys. Rev. E* **93**, 012107 (2016).
- [209] H. Z. Shen, D. X. Li, S. L. Su, Y. H. Zhou, and X. X. Yi, Exact non-Markovian dynamics of qubits coupled to two interacting environments, *Phys. Rev. A* **96**, 033805 (2017); H. Z. Shen, S. L. Su, Y. H. Zhou, and X. X. Yi, Non-Markovian quantum Brownian motion in one dimension in electric fields, *ibid.* **97**, 042121 (2018).
- [210] H. Z. Shen, C. Shang, Y. H. Zhou, and X. X. Yi, Unconventional single-photon blockade in non-Markovian systems, *Phys. Rev. A* **98**, 023856 (2018); H. Z. Shen, Q. Wang, J. Wang, and X. X. Yi, Nonreciprocal unconventional photon blockade in a driven dissipative cavity with parametric amplification, *ibid.* **101**, 013826 (2020).
- [211] Q. T. Xie, S. Cui, J. P. Cao, L. Amico, and H. Fan, Anisotropic Rabi model, *Phys. Rev. X* **4**, 021046 (2014).
- [212] X. Y. Chen, L. W. Duan, D. Braak, and Q. H. Chen, Multiple ground-state instabilities in the anisotropic quantum Rabi model, *Phys. Rev. A* **103**, 043708 (2021).
- [213] M. A. Rodríguez, P. Tempesta, and P. Winternitz, Reduction of superintegrable systems: The anisotropic harmonic oscillator, *Phys. Rev. E* **78**, 046608 (2008).
- [214] S. Nakajima, Perturbation theory in statistical mechanics, *Adv. Phys.* **4**, 363 (1955).
- [215] H. Fröhlich, Theory of the superconducting state. I. The ground state at the absolute zero of temperature, *Phys. Rev.* **79**, 845 (1950).
- [216] H. Fröhlich, Interaction of electrons with lattice vibrations, *Proc. R. Soc. London A* **215**, 291 (1952); Q. Ai, Y. Li, H. Zheng, and C. P. Sun, Quantum anti-Zeno effect without rotating wave approximation, *Phys. Rev. A* **81**, 042116 (2010); H. Zheng, Dynamics of a two-level system coupled to Ohmic bath: A perturbation approach, *Eur. Phys. J. B* **38**, 559 (2004).
- [217] Z. G. Lü and H. Zheng, Quantum dynamics of the dissipative two-state system coupled with a sub-Ohmic bath, *Phys. Rev. B* **75**, 054302 (2007).
- [218] M. H. Fischer, M. Maksymenko, and E. Altman, Dynamics of a many-body-localized system coupled to a bath, *Phys. Rev. Lett.* **116**, 160401 (2016).
- [219] V. R. Overbeck and H. Weimer, Time evolution of open quantum many-body systems, *Phys. Rev. A* **93**, 012106 (2016).
- [220] M. V. Medvedyeva, T. Prosen, and M. Žnidarič, Influence of dephasing on many-body localization, *Phys. Rev. B* **93**, 094205 (2016).
- [221] M. Metcalf, J. E. Moussa, W. A. de Jong, and M. Sarovar, Engineered thermalization and cooling of quantum many-body systems, *Phys. Rev. Res.* **2**, 023214 (2020).
- [222] X. S. Xu, J. Thingna, C. Guo, and D. Poletti, Many-body open quantum systems beyond Lindblad master equations, *Phys. Rev. A* **99**, 012106 (2019).
- [223] J. Lebreuilly, A. Biella, F. Storme, D. Rossini, R. Fazio, C. Ciuti, and I. Carusotto, Stabilizing strongly correlated photon fluids with non-Markovian reservoirs, *Phys. Rev. A* **96**, 033828 (2017).

- [224] J. Li, S. Y. Zhu, and G. S. Agarwal, Magnon-photonphonon entanglement in cavity magnomechanics, *Phys. Rev. Lett.* **121**, 203601 (2018).
- [225] X. F. Zhang, C. L. Zou, L. Jiang, and H. X. Tang, Cavity magnomechanics, *Sci. Adv.* **2**, e1501286 (2016).
- [226] M. Amazioug, S. K. Singh, B. Teklu, and M. Asjad, Coherent feedback control of quantum correlations in cavity magnomechanical system with magnon squeezing, [arXiv:2302.08567](https://arxiv.org/abs/2302.08567).
- [227] J. Li, S. Y. Zhu, and G. S. Agarwal, Squeezed states of magnons and phonons in cavity magnomechanics, *Phys. Rev. A* **99**, 021801(R) (2019).
- [228] K. Ullah, M. T. Naseem, and Ö. E. Müstecaplıoğlu, Tunable multiwindow magnomechanically induced transparency, Fano resonances, and slow-to-fast light conversion, *Phys. Rev. A* **102**, 033721 (2020).
- [229] S. Vashahri-Ghamsari, Q. Lin, B. He, and M. Xiao, Magnomechanical phonon laser beyond the steady state, *Phys. Rev. A* **104**, 033511 (2021).
- [230] B. Hussain, S. Qamar, and M. Irfan, Entanglement enhancement in cavity magnomechanics by an optical parametric amplifier, *Phys. Rev. A* **105**, 063704 (2022).
- [231] W. Y. Qiu, X. H. Cheng, A. X. Chen, Y. H. Lan, and W. J. Nie, Controlling quantum coherence and entanglement in cavity magnomechanical systems, *Phys. Rev. A* **105**, 063718 (2022).
- [232] B. Sarma, T. Busch, and J. Twamley, Cavity magnomechanical storage and retrieval of quantum states, *New J. Phys.* **23**, 043041 (2021).
- [233] J. Li and S. Y. Zhu, Entangling two magnon modes via magnetostrictive interaction, *New J. Phys.* **21**, 085001 (2019).
- [234] W. Zhang, T. Wang, X. Han, S. Zhang, and H. F. Wang, Quantum entanglement and one-way steering in a cavity magnomechanical system via a squeezed vacuum field, *Opt. Express* **30**, 10969 (2022).
- [235] C. Kittel, Interaction of spin waves and ultrasonic waves in ferromagnetic crystals, *Phys. Rev.* **110**, 836 (1958).
- [236] M. S. Ebrahimi, A. Motazedifard, and M. B. Harouni, Single-quadrature quantum magnetometry in cavity electromagnonics, *Phys. Rev. A* **103**, 062605 (2021).
- [237] C. Kong, H. Xiong, and Y. Wu, Magnon-induced nonreciprocity based on the magnon Kerr effect, *Phys. Rev. Appl.* **12**, 034001 (2019); J. Y. Sun and H. Z. Shen, Photon blockade in non-Hermitian optomechanical systems with nonreciprocal couplings, *Phys. Rev. A* **107**, 043715 (2023); C. Shang, H. Z. Shen, and X. X. Yi, Nonreciprocity in a strongly coupled three-mode optomechanical circulatory system, *Opt. Express* **27**, 25882 (2019); J. Wang, Q. Wang, and H. Z. Shen, Nonreciprocal unconventional photon blockade with spinning atom-cavity, *Europhys. Lett.* **134**, 64003 (2021).
- [238] A. Gloppe, R. Hisatomi, Y. Nakata, Y. Nakamura, and K. Usami, Resonant magnetic induction tomography of a magnetized sphere, *Phys. Rev. Appl.* **12**, 014061 (2019).
- [239] R. Hisatomi, A. Osada, Y. Tabuchi, T. Ishikawa, A. Noguchi, R. Yamazaki, K. Usami, and Y. Nakamura, Bidirectional conversion between microwave and light via ferromagnetic magnons, *Phys. Rev. B* **93**, 174427 (2016).
- [240] A. Osada, R. Hisatomi, A. Noguchi, Y. Tabuchi, R. Yamazaki, K. Usami, M. Sadgrove, R. Yalla, M. Nomura, and Y. Nakamura, Cavity optomagnonics with spin-orbit coupled photons, *Phys. Rev. Lett.* **116**, 223601 (2016).
- [241] A. Osada, A. Gloppe, R. Hisatomi, A. Noguchi, R. Yamazaki, M. Nomura, Y. Nakamura, and K. Usami, Brillouin light scattering by magnetic quasivortices in cavity optomagnonics, *Phys. Rev. Lett.* **120**, 133602 (2018).
- [242] R. Hisatomi, A. Noguchi, R. Yamazaki, Y. Nakata, A. Gloppe, Y. Nakamura, and K. Usami, Helicity-changing Brillouin light scattering by magnons in a ferromagnetic crystal, *Phys. Rev. Lett.* **123**, 207401 (2019).
- [243] S. P. Wolski, D. Lachance-Quirion, Y. Tabuchi, S. Kono, A. Noguchi, K. Usami, and Y. Nakamura, Dissipation-based quantum sensing of magnons with a superconducting qubit, *Phys. Rev. Lett.* **125**, 117701 (2020).
- [244] Y. P. Wang, G. Q. Zhang, D. K. Zhang, X. Q. Luo, W. Xiong, S. P. Wang, T. F. Li, C. M. Hu, and J. Q. You, Magnon Kerr effect in a strongly coupled cavity-magnon system, *Phys. Rev. B* **94**, 224410 (2016).
- [245] K. I. Uchida, H. Adachi, T. Ota, H. Nakayama, S. Maekawa, and E. Saitoh, Observation of longitudinal spin-Seebeck effect in magnetic insulators, *Appl. Phys. Lett.* **97**, 172505 (2010).
- [246] C. Safranski, I. Barsukov, H. K. Lee, T. Schneider, A. A. Jara, A. Smith, H. Chang, K. Lenz, J. Lindner, Y. Tserkovnyak, M. Wu, and I. N. Krivorotov, Spin caloritronic nano-oscillator, *Nat. Commun.* **8**, 117 (2017).
- [247] J. Holanda, O. A. Santos, R. L. Rodríguez-Suárez, A. Azevedo, and S. M. Rezende, Simultaneous spin pumping and spin Seebeck experiments with thermal control of the magnetic damping in bilayers of yttrium iron garnet and heavy metals: YIG/Pt and YIG/IrMn, *Phys. Rev. B* **95**, 134432 (2017).
- [248] G. Q. Zhang, Y. M. Wang, and W. Xiong, Detection sensitivity enhancement of magnon Kerr nonlinearity in cavity magnonics induced by coherent perfect absorption, *Phys. Rev. B* **107**, 064417 (2023).
- [249] G. Q. Zhang and J. Q. You, Higher-order exceptional point in a cavity magnonics system, *Phys. Rev. B* **99**, 054404 (2019).
- [250] G. Q. Zhang, Z. Chen, D. Xu, N. Shammah, M. Y. Liao, T. F. Li, L. M. Tong, S. Y. Zhu, F. Nori, and J. Q. You, Exceptional point and cross-relaxation effect in a hybrid quantum system, *PRX Quantum* **2**, 020307 (2021); Q. Wang, J. Wang, H. Z. Shen, S. C. Hou, and X. X. Yi, Exceptional points and dynamics of a non-Hermitian two-level system without PT symmetry, *Europhys. Lett.* **131**, 34001 (2020); T. Z. Luan, J. Y. Sun, and H. Z. Shen, Dynamical approach to shortcuts to adiabaticity for general two-level non-Hermitian systems, *ibid.* **142**, 58001 (2023); Y. H. Zhou, H. Z. Shen, X. Y. Zhang, and X. X. Yi, Zero eigenvalues of a photon blockade induced by a non-Hermitian Hamiltonian with a gain cavity, *Phys. Rev. A* **97**, 043819 (2018).
- [251] A. Wallraff, D. I. Schuster, A. Blais, L. Frunzio, J. Majer, M. H. Devoret, S. M. Girvin, and R. J. Schoelkopf, Approaching unit visibility for control of a superconducting qubit with dispersive readout, *Phys. Rev. Lett.* **95**, 060501 (2005).
- [252] R. Vijay, C. Macklin, D. H. Slichter, S. J. Weber, K. W. Murch, R. Naik, A. N. Korotkov, and I. Siddiqi, Stabilizing Rabi oscillations in a superconducting qubit using quantum feedback, *Nature (London)* **490**, 77 (2012).
- [253] S. Filipp, P. Maurer, P. J. Leek, M. Baur, R. Bianchetti, J. M. Fink, M. Göppl, L. Steffen, J. M. Gambetta, A. Blais, and A. Wallraff, Two-qubit state tomography using a joint dispersive readout, *Phys. Rev. Lett.* **102**, 200402 (2009).

- [254] M. Schreier, T. Chiba, A. Niedermayr, J. Lotze, H. Huebl, S. Geprägs, S. Takahashi, G. E. W. Bauer, R. Gross, and S. T. B. Goennenwein, Current-induced spin torque resonance of a magnetic insulator, *Phys. Rev. B* **92**, 144411 (2015).
- [255] Y. Tserkovnyak, A. Brataas, G. E. W. Bauer, and B. I. Halperin, Nonlocal magnetization dynamics in ferromagnetic heterostructures, *Rev. Mod. Phys.* **77**, 1375 (2005).